Contrasting Paleoproterozoic granitoids in the Kerdous, Tagragra d'Akka, Agadir-Melloul and Iguerda inliers (western Anti-Atlas, Morocco)

Olivier Blein, Philippe Chevremont, Thierry Baudin, Ahmid Hafid, Hassan Admou, Abderrahmane Soulaimani, Hassan Ouanaimi, Mohamed Bouabdelli, Dominique Gasquet, Maxime Padel

Contrasting Paleoproterozoic granitoids in the Kerdous, Tagragra d'Akka, Agadir-Melloul and Iguerda inliers (western Anti-Atlas, Morocco)

Olivier BLEIN[1], Philippe CHEVREMONT[1], Thierry BAUDIN[1], Ahmid HAFID[2], Hassan ADMOU[3], Abderrahmane SOULAIMANI[3], Hassan OUANAIMI[4], Mohamed BOUABDELLI[5], Dominique GASQUET[6], Maxime PADEL[1]

[1] BRGM, 3 av. Claude Guillemin, BP 36009, 45060 Orléans Cédex, France; o.blein@brgm.fr

ORCID : 0000-0003-3514-9641

[2] Department of Geology, Faculty of Sciences & Technics Guéliz, Cadi Ayyad University, P.O. Box 549, Marrakech 40005, Morocco

[3] Department of Geology, Faculty of Sciences-Semlalia, Cadi Ayyad University, P.O. Box 2390, Marrakech 40005, Morocco

[4] Department of Geology, ENS, Cadi Ayyad University, P.O. Box 2400, Marrakech 40005, Morocco

[5] GEODE Terre et Patrimoine, B.P. 7004, 40014 Marrakech, Morocco.

[6] Université Savoie Mont Blanc, Laboratoire EDYTEM, UMR 5204 CNRS, Bâtiment Pole Montagne, Campus Scientifique, 73376 Le Bourget du Lac, France.

Keywords. Anti-Atlas, Eburnean, Paleoproterozoic, Granite, Geochemistry, U-Pb Geochronology.

ABSTRACT

The northern margin of the West African Craton is characterized by Paleoproterozoic siliciclastic sediments intruded by ca. 2.1-2.0 Ga Eburnean granitoids. New geochronological data highlight the occurrence of a Rhyacian (2.10 Ga) tonalitic to trondhjemitic magmatic suite, following a coeval Orosirian (2.040-2.035 Ga) magmatic suite composed of calc-alkaline diorites, mesocratic granites and leucogranites.

Whole-rock major and trace element compositions indicate that: (i) the Rhyacian tonalites and trondhjemites suggest a subduction environment, an island-arc arc or an active continental margin; (ii) the Orosirian plutonic rocks show a geochemical heterogeneity; (iii) the chemical features of diorites correspond to calc-alkaline M-type suites; (iv) granodiorites and granites are typical calc-alkaline I-type granitoids, and (iv) leucogranites, with peraluminous composition, reflect a crustal melting.

While the Rhyacian magmatic event indicates a subduction environment, the Orosirian magmatic event is more complex, and the geochemical signatures imply involvement of mantellic magmas and crustal melting. The contemporaneity of these Orosirian magmatic suites and their siliciclastic sedimentary host-rocks suggest a back-arc geodynamic context, similar to what was described in the Reguibat Rise, Mauritania.

1. Introduction

In the northern West African Craton (nWAC), the Anti-Atlas (AA) inliers are characterised by a Precambrian basement unconformably overlied by late Ediacaran to Paleozoic sedimentary rocks (Bas Drâa, Ifni, Kerdous, Tagragra d'Akka, Igherm, Iguerda, Sirwa, Zenaga, Bou Azzer-El Graara, Saghro and Ougnat). The lithostratigraphy of these inliers allows to distinguish three main structural domains (Choubert, 1947, 1952) (**Fig. 1**): (1) the western AA, south of the Anti-Atlas major fault (AAMF) in the Bas Drâa, Ifni, Kerdous, Tagragra d'Akka, Igherm, Agadir Melloul, Iguerda and Zenaga inliers; (2) the central AA along the AAMF in the Sirwa and Bou Azer inliers; and (3) the eastern AA, north of the AAMF in the Saghro and Ougnat inliers.

The oldest rocks of the Anti-Atlas, exposed in its western inliers, encompass old metasedimentary rocks intruded by 2 Ga Eburnean granitoids (Ait Malek et al., 1998; Gasquet et al., 2004; Barbey et al., 2004; O'Connors et al., 2010). Conversely, Eburnean basement exposures are lacking in the pan-African areas along the Central AA suture and in the northeastern Saghro-Ougnat and High Atlas

massifs. It is however important to remember that the cratonic basement may extend beneath these northern areas as indicated by the presence of inherited Paleoproterozoic zircon in the Neoproterozoic magmatic rocks (Gasquet et al., 2005; Baidada et al., 2019).

The western AA inliers are characterized by three major geological events: (1) a ca. 2.1-2.0 Ga Paleoproterozoic Eburnean event (Aït Malek et al., 1998; Thomas et al., 2002; Gasquet et al., 2004; Mortaji et al., 2000; O'Connor et al., 2010); (2) a passive margin sequence deposited during rifting and break-up of the *n*WAC which has long been ascribed to the Tonian-Cryogenian (Clauer, 1976; Thomas et al., 2004), but recently constrained between 1.8 and 1.7 Ga based on their detrital zircon content (Abati et al., 2010; Soulaimani et al., 2019), on 1710 Ma age (U–Pb on baddeleyite) of basic sills (Ikenne et al., 2017; Youbi et al., 2013) and ca. 1630 Ma (U–Pb zircon; Aït Lahna et al., 2020); and (3) a large volume of volcanic and volcano-sedimentary Ediacaran deposits (Thomas et al., 2002; Gasquet et al., 2005, 2008; Benziane, 2007; Blein et al., 2014a, 2014b).

Paleoproterozoic basement consists of several sequences of siliciclastic sedimentary deposits recrystallized under low-grade to partial melting metamorphic conditions, and intruded by Paleoproterozoic syn- to late kinematic granites. Using geochemical data, two Paleoproterozoic plutonic units have been recognized (**Fig.1**): calc-alkaline and peraluminous rocks.

In Bas Drâa and Tagragra of Akka inliers, the calc-alkaline unit consists of diorites, monzo-gabbro-diorites, granodiorites and monzogranites. Their chemical features correspond to calc-alkaline I-type, suggesting a lower crustal, or mantle origin with variable contamination by crustal material (Ikenne, 1997; Mortaji et al., 2000; O'Connor et al., 2010). The Peraluminous plutonic rocks are granodiorites, granites and leucogranites of crustal origin (Mortaji et al., 2000). In Zenaga inlier, Paleoproterozoic granitoids are represented by a calc-alkaline suite of granodiorites and granites reflecting a lower crustal or mantle origin with variable contamination by crustal material, and by peraluminous granodiorites, and monzogranites of crustal origin (Thomas et al., 2002; Ennih and Liégois, 2008).

Geological mapping in Kerdous, Tagragra d'Akka, Agadir-Melloul and Iguerda inliers, within the framework of the Moroccan National Project of Geological Mapping (1/50 000 scale sheet maps of Sidi Bou'Addi, Tamazrar, Awkarda, Tlatat Ida Gougmar, Agadir Melloul, Assaragh, Ighriy and Tabadrist) gave opportunities to acquire new field, geochemical and geochronological data on the Paleoproterozoic plutonic rocks (**Fig. 1**). The aims of this paper are: (i) to re-evaluate the

Paleoproterozoic plutonic rocks, (ii) to present new geochemical data, (iii) to discuss the geodynamical evolution of the *n*WAC during Eburnean orogeny times, and (iv) to clarify the timing of Paleoproterozoic plutonic suites based on new geochronological data.

2. Regional setting

Five main lithological units were identified in the Tagragra d'Akka, Kerdous, Agadir-Melloul and Iguerda inliers corresponding to major geodynamic events composed of (1) oldest metasedimentary schists, (2) two plutonic suites, both constituting the Paleoproterozoic basement which is also crosscut by numerous mafic and felsic dikes, quartz veins and rare dacite dikes, (3) Paleoproterozoic to Neoproterozoic sedimentary cover, (4) Ediacaran volcano-sedimentary and volcanic rocks, and (5) late Ediacaran and early Cambrian sediments.

2.1. Paleoproterozoic basement

The metasedimentary schists derive from pelites and fine-grained sandstones with interbedded volcanic layers. Felsic metatuffs have been dated at 2072 ± 8 Ma by Walsh et al. (2002) in the Tagragra de Tata inlier. The metasedimentary serie has been affected by a first Eburnean phase of folding which is prior to the plutonic intrusions. This is particularly demonstrative in the Tagragra d'Akka inlier where hectometric relicts of vertical isoclinal foldings are still preserved (**Fig. 2A**). The latter have been then transposed by regional shear corridors parallel to the previous fold axis, developing the main regional schistosity (Gasquet et al., 2001). These structures are observed in all Anti-Atlas inliers, where they are associated with metamorphic conditions ranging from greenschist to amphibolitic facies with local migmatites. Both deformation and metamorphism predate plutonic intrusions though this magmatism could be part of the last stage of the same Eburnean geodynamic event.

Two Paleoproterozoic plutonic events have been recognized: i) a first calc-alkaline suite of diorites, monzogabbros, granodiorites and monzogranites reflecting a lower crustal or mantle origin with variable contamination by crustal material; and ii) a second peraluminous suite of granodiorites, granites and leucogranites (Mortaji et al., 2000). In Bas Drâa and Tagragra of Akka Inliers (Ikenne, 1997; Mortaji et al., 2000) the calc-alkaline unit consists of diorites, monzodiorites, granodiorites and monzoranites. Their chemical affinities are those of calc-alkaline I-type suggesting a lower crustal, or mantle, origin with variable contamination by crustal material. In Zenaga inliers (Thomas et al., 2002;

105 Ennih and Liégeois, 2008), medium-K calc-alkaline intrusions are qualified as Azguemerzi Type,
106 consisting of quartz-monzodiorite, granodiorites and monzogranites with geochemical features of
107 subduction-related magmas as a result of differentiation from a mantle-derived calc-alkaline and/or
108 mafic magma. These granitoïds have been dated at 2037 ± 7 Ma, 2037 ± 9 Ma and 2032 ± 5 Ma
109 (Thomas et al., 2002). The peraluminous group, consisting of muscovite or two-mica granites,
110 leucogranites and granodiorites, was generated in a syn-collisional environment from a crustal source
111 (Thomas et al., 2002; Gasquet et al., 2008; Ennih and Liégeois, 2008).

112 **2.2. Proterozoic passive margin**

113 From late Paleoproterozoic, a passive margin was established along the northern edge of the West
114 African Craton. It overlies the basement rocks with a strong angular unconformity. The sedimentary
115 sequence, associated to this passive margin, is named differently according to the areas: the Lkest-
116 Taghdout Group in the Zenaga, Agadir-Melloul and Iguerda inliers (Thomas et al., 2002; Blein et al.,
117 2013; Chèvremont et al., 2013; Soulaimani et al., 2013), the Lkest Group in the Kerdous (BGS, 2001)
118 or the Tizi n'Taghatine Group in the central Anti-Atlas (Bouougri and Saquaque, 2004). These
119 equivalent groups are composed from bottom to top of thick layered quartzites, stromatolitic
120 carbonates and sandy-pelitic beds. The basal quartzite level unconformably overlies the
121 Paleoproterozoic basement (Chèvremont et al., 2013). This transgressive serie have been long
122 considered as Neoproterozoic in age, pointing out the start of the Bou Azzer ocean aperture during
123 Tonian-Cryogenian (Clauer, 1976; Bouougri and Saquaque, 2004; Thomas et al., 2004). Since few
124 years new datations carried out on abundant dykes and sills of dolerites and gabbros, crosscutting this
125 group provided ages older than expected i.e. between 1.8 and 1.7 Ga based on their detrital zircon
126 content (younger grains dated at 1.8 Ma; Abati et al., 2010; Soulaimani et al., 2019), on their
127 intersection by mafic sills dated at ca. 1710 Ma (U–Pb on baddeleyite; Ikenne et al., 2017; Youbi et al.,
128 2013) and ca. 1630 Ma (U–Pb zircon; Kouyate et al., 2013; Aït Lahna et al., 2020). The deposit of
129 these transgressive sedimentary groups (Lkest-Taghdout) should thus date from the late
130 Paleoproterozoic time.

131 Likewise, the previously admitted nonexistence of Mesoproterozoic magmatic events or rocks
132 (between 1.7 and 1.0 Ga, Ennih and Liégeois, 2001) has being called into question by the ages
133 determined on the Bas Drâa mafic dykes at 1416-1380 Ma by El Bahat et al. (2013).

2.3. Cryogenian-Pan African cycle

In contrast with the Central and eastern AA, geological markers of the Pan-African cycle in the Western AA are not obvious, except the widespread Ediacaran magmatic event. The Tonian platform established at the northern edge of the WAC is restricted to Tachdamt Bleïda sequences along the Central AA Pan-African Suture (Letsch 2018; Bouougri et al., 2020). Only Tonian dykes crosscut Paleoproterozoic basement of western AA inliers (Kouyaté et al., 2013; Youbi et al., 2013).

The same is true for the Cryogenian Bou Azzer Group including accreting oceanic island-arc terrane (D'Lemos et al., 2006; Thomas et al., 2002; Blein et al., 2014a; Triantafyllou et al., 2016; 2018; 2020; Errami et al., 2020), Cryogenian dismembered oceanic supra-subduction ophiolite (Leblanc, 1975; Bodinier et al., 1984; Saquaque et al., 1989; Bousquet et al., 2008; Walsh et al., 2012; Blein et al., 2014a; El Hadi et al., 2010; Soulaimani et al., 2006; 2018; Hodel et al., 2020), and volcano-sedimentary succession filling arc-related basins (Saquaque et al., 1989; Hefferan et al., 2000; Inglis et al., 2005; Blein et al., 2014a), which exposures are restricted to the Bou Azzer and Sirwa inliers.

The occurrence of the Pan-African tectonic events in the Western AA is still open to discussion. In the Kerdous inlier the Jbel Lkest quartzite are affected by a severe shear deformation, coherent with a dextral transpressive shear tectonics (Hassenforder, 1987).

2.4. Ediacaran-Cadomian magmatic events

The Ediacaran formations can be are divided into three groups: i) the Saghro Group (central and Eastern AA); ii) the Anezi series (western AA), Tiddiline and Jbel Wawkida groups (central AA), and the Bou Salda or Mgouna Group (eastern AA); and iii) the Ouarzazate Group.

The folded series of the Saghro Group extend from Sirwa to Saghro and Ougnat massifs in the Eastern Anti-Atlas and in the Proterozoic outcrops of the High Atlas (Ouguir et al. 1996; Thomas et al., 2002; Fekkak et al., 2003; Eddif et al., 2007; Michard et al., 2017). The Saghro Group has been considered as northern Cryogenian distal equivalent to the pre-Pan-African platform margin sequences (Saquaque et al., 1992; Ouguir et al., 1996; Thomas et al., 2002), deposited in an extensional back-arc environment (Ouguir et al., 1996).

The Anezi-Tiddiline-Bou Salda Group consists of a thick volcano-sedimentary formation deposed in very subsident troughs probably linked to a transtensive tectonics (Errami et al., 2009; Blein et al.,

2014b). The ages obtained from rhyolites and ignimbrites of the Bou Salda and Tiddiline groups range between 605 and 607 Ma (Thomas et al., 2002; Blein et al., 2014b; Errami et al., 2020). These deep basins have been inverted during the latest Panafrican compressive event leading to the formation of reliefs and their rapid following erosion, around 580 Ma ago. It's on this unconformity surface that the Ouarzazate Group deposed. For instance, in the Bou Azzer inlier, folded ignimbrite of the Tiddiline Group is unconformably overlain by ignimbrite of the Ouarzazate Group (Blein et al., 2014b).

The Ouarzazate Group corresponds to large volume of volcanic, pyroclastic, and sub-volcanic plutonic rocks. These volcanic sequences are characterized by abundant intermediate to felsic pyroclastic rocks, with rare basaltic flows. These rocks belong to high-K calc-alkaline to shoshonitic suites and are essentially, classified as I- and S-type magmas, and locally, some plutons are composed of A-type granites (Thomas et al., 2002; El Baghdadi et al., 2003; Gasquet et al., 2005, 2008; Errami et al., 2009; Toummite et al., 2012; Walsh et al., 2012; Blein et al., 2014a; Baidada et al., 2017; Belkacim et al., 2017). Principal U-Pb zircon ages from the Ouarzazate Group range between 575 and 545 Ma (Hawkins et al., 2001; Cheilletz et al., 2002; Walsh et al., 2002; Gasquet et al., 2005; Blein et al., 2014a, 2014b; Errami et al., 2020). In the Central Atlas, the important thickness variations of the volcaniclastic Ouarzazate deposits are controlled, at the first order, by an accented paleogeography (Blein et al., 2014a). Moreover, the successive volcaniclastic deposits are also submitted to a syn-sedimentary tectonic event such as NW-SE striking folding and NE-SW faulting (Blein et al., 2014a).

This late Ediacaran event is interpreted as subduction-related (Bajja, 1998; El Baghdadi et al., 2003; Benziane, 2007; Walsh et al., 2012), or post-collisional with respect to the arc-continental collision of the main Pan-African event (Thomas et al., 2002; Gasquet et al., 2005, 2008; Toummite et al., 2012; Blein et al., 2014a, b).

Blein et al. (2014b) consider the possibility of a subduction beneath the WAC margin at about 630-585 Ma, the cessation of the subduction between 580 and 575 Ma, and the development of an upper Ediacaran felsic magmatism resulting from partial melting of continental crust, attributed to asthenospheric rise.

Andesitic basalts and alkaline to tholeiitic trends characterize the volcanic rocks in the overlying Taroudant Group (Gasquet et al., 2005, 2008). Initially highly potassic and calc-alkaline, the volcanic rocks evolved to more alkaline compositions during deposition of the overlying Adoudounian

sedimentary rocks (Choubert, 1958) at the Ediacaran-Cambrian transition (Gasquet et al., 2005; Benziane, 2007; Alvaro et al., 2008; Ezzouhairi et al., 2008).

2.5. Late Ediacaran to Cambrian sedimentary rocks

In the Anti-Atlas, the transition between the Ouarzazate Group and the Adoudou Formation (late Ediacaran – Early Cambrian sedimentary cover) is described overall like an unconformity, locally angular (Hassenforder, 1987), or erosional in Jbel Saghro (Benziane et al., 1983), but is also described as progressive passage in the western Anti-Atlas (Piqué et al., 1999; Soulaimani et al., 2003; Alvaro, 2020).

The Ouarzazate Group is characterized by a pre-Cambrian deformation, which is contemporaneous of the volcano-clastic rocks deposition (Blein et al., 2014a). While the oldest deposits are folded, the most recent deposits, which are in continuity with the late Ediacaran and Cambrian sedimentary cover, are not affected by this pre-Cambrian deformation except for a light Variscan deformation. This syn-sedimentary deformation explains why the oldest deposits of the Ouarzazate Group are covered in discordance by Cambrian sediments and the most recent deposits in concordance.

The Ediacaran-Cambrian transition is characterized by a carbonate-dominated succession, the Taroudannt Group (Choubert, 1952; 1953a, b). This group is composed by the mainly carbonated Adoudou Formation and the mixed (terrigenous-carbonated) Taliwine Formation, which becomes dominant carbonate westward while it is exclusively terrigenous further east, in the central Anti-Atlas.

The Adoudou Formation is composed of shallow carbonate deposits with structures of microbial origin. It fits into a widespread subsidence context responsible for the progressive flooding of the Anti-Atlas basin, which promotes the installation of a first peritidal carbonate platform of high extension (Boudda et al., 1979; Geyer, 1990; Benssaou and Hamoumi, 2001; Alvaro et al., 2005). An early U/Pb date of 529 ± 3 Ma from the Boho volcano (Ducrot and Lancelot, 1977) and of 531 ± 5 Ma from the Aghbar trachyte sill (Gasquet et al., 2005) suggest that deposition of the uppermost part of the Adoudou Formation took place in the earliest Cambrian. Recent U-Pb age of 541 ± 6 Ma from a volcanic breccia at the base of the Adoudou Formation (Blein et al., 2014b) suggests that deposition of the Adoudou Formation took place at the limit between Ediacaran and Cambrian.

The boundary between the Adoudou and Taliwine formations is marked by a rapid but gradual disappearance of dolomite layers in favor of silty clay deposits, displaying a purplish red color refered

as “lie de vin”. Volcanic ashes intercalated within Taliwine Formation have been dated at 521 ± 7 Ma and 522 ± 2 Ma (Compston et al., 1992; Landing et al., 1998; Maloof et al., 2005).

3. Paleoproterozoic granitoids

According to their mineralogical composition we distinguished within the Paleoproterozoic plutonic rocks inventoried four main magmatic suites: i) tonalites and trondhjemites; ii) quartz-diorites; iii) calc-alkaline granodiorites and monzogranites; and iv) leucogranites.

3.1. Diorites

Diorites, observed essentially in the Iguerda and Agadir-Melloul Imoula inliers (**Fig. 3**), are represented by three types of plutonic rocks: i) a fine to medium-grained quartz-monzodiorite; ii) an orbicular diorite; and iii) a medium-grained quartz-diorite to tonalite.

Discovered Agard (1952), the *quartz-monzodiorite* of Tayfast extends on a length from ca. 2 km, located in the south-west Tayfast douar. It is a mesocratic to melanocratic rock of equigranular grained texture, with fine to medium sized grain (≤ 4 mm), containing plagioclase, quartz, amphibole, epidote and biotite. The quartz-monzodiorite of Tayfast is intrusive in the metasedimentary basement. This diorite shows a hypidiomorphic granular texture medium-grained (<3 mm). It consists of sub-automorphic or automorphic plagioclase, xenomorphic amphibole, biotite and accessory minerals such as leucoxene, zircon, apatite, Fe and/or Ti oxides, allanite.

The *orbicular diorite* of Tayfast outcrops in the form of a small lenticular body, wedged in an albitic granite, sub-leucocratic and pseudo-porphyritic, with biotite. The orbicules are roughly elliptically shaped with a major axis between 1 and 13 cm, with an average of 4 to 5 cm. The external aureoles, with a predominantly radial texture, have a width from 5 to 6 mm broad and are characterized by their dark color, due to equal amounts of plagioclase and amphibole with lesser amounts of clinopyroxene, biotite and magnetite. The core of the orbicules and the surrounding matrix rock has a hypidiomorphic medium-grained texture, strongly obliterated by hydrothermal alteration. The core of the orbicules is polycrystalline and corresponds to a quartz-diorite composed of plagioclase, amphibole, quartz, with small amounts of K-feldspar, clinopyroxene and accessories, mainly magnetite.

These types of orbicular structures have been carefully reviewed by Leveson (1966). Although their magmatic origin is not questioned, the genesis of orbicular rocks is complex and no single hypothesis

provides a general explanation for their origin and numerous mechanisms have been proposed, reflecting the diversity of the orbicular settings and habits (see Decitre et al, 2002; Diaz-Alvarado et al., 2017 and references therein). The growth of shells corresponds to the rapid crystallisation of immiscible supersatured magmas convecting around nuclei or the orbicular structure is controlled by adiabatic undercooling. The growth of successive shells may be also related to rapid diffusion-controlled crystallisation of the different components within the melt or are formed by rhythmic supersaturation and crystallisation from a gel in a manner analogous to Liesegang rings (Leveson, 1966) or from magma during differentiation. The "magma" in which orbicules develop must have the diffusive and rheological properties of a concentrated macromolecular paste or gel of mixed hydrosilicates. The most common mechanism proposed by the authors involves diffusion. The crucial factor is the feeding of the "orbicular melt" in "cold" seeds together with a restricted range (around the liquidus) of the melt temperature, which is a severe limiting condition which explain the paucity of orbicular rocks in the geological record is readily explained.

Quartz-diorites constitute small bodies, dispersed and enclaved in granitic massifs. The most important bodies are located in the westernmost part of the Agadir-Melloul inlier. This igneous rock shows a porphyroclastic texture, with the composition of a tonalite with biotite. It contains, by order of decreasing abundance, the following minerals: sub-automorphic plagioclase, more or less sericitized; quartz in very xenomorphic spaces, presenting multiple sub-grains; xenomorphic orthoclase feldspar, significantly less abundant than plagioclase. Brown biotite is presented in small directed, isolated strip, and altered by a local, partial or total chloritisation. Accessory minerals are apatite and zircon.

3.2. Tonalites and trondhjemites

Tonalites and trondhjemites (or leucotonalites) are essentially observed in the northern part of the Tazeroualt massif in the Kerdous inlier (**Fig. 2B**). These granitoids have hypidiomorphic granular texture, medium to coarse-grained, never porphyritic, and are intrusive within the metasedimentary basement.

Biotite-amphibole tonalite is mesocratic with a well-defined planar fabric. In thin section, tonalite displays a hypidiomorphic to grano-lepido-nematoblastic texture with a heterogeneous grain size (2 to 12 mm). K-feldspars are lacking, and plagioclases are sub-euhedral to euhedral, with biotite

inclusions. Biotites and green amphiboles (hornblende) are abundant, and associated with accessory minerals such as epidote, zircon, apatite, and Fe and/or Ti oxides.

Two-mica trondhjemite is easily distinguishable of the previous tonalite by a lighter color: in a quartzo-feldspathic white background are scattered small elongated biotite clusters defining a clear planar fabric less marked than in the mesocratic tonalite. In thin section, trondhjemite shows a hypidiomorphic to slightly myrmekitic texture with a grain size (1 to 5 mm) more homogeneous than in mesocratic tonalite.

3.3. Granodiorites and monzogranites

Granodiorites and monzogranites have been observed in the Kerdous, the Tagragra d'Akka, the Agadir-Melloul and Iguerda inliers (**Fig. 2A, C**). This suite is represented by three main types of granites: i) a mesocratic granodiorite; ii) a mesocratic porphyritic monzogranite; and iii) a mesocratic medium-grained monzogranite.

Mesocratic granodiorite is more abundant than diorites, but with a heterogeneous geographic distribution. Indeed, it outcrops in the eastern part of the Tagragra d'Akka (**Fig. 2A**), constitutes a small massif in the northern part of the Agadir Melloul-Imoula inlier while it is predominant in the eastern half of the Ti-n-Maliz-Tamjircht inlier (**Fig. 3**). It is a mesocratic porphyritic medium to coarse-grained granodiorite composed of quartz, plagioclase, K-feldspar, and biotite more or less chloritized. Length of feldspar phenocrysts generally ranges between 1 and 2 cm and rarely reaches 5 cm.

Mesocratic porphyritic monzogranite constitutes the predominant igneous rock in the eastern part of the Tagragra d'Akka (**Fig. 2A**), the south-western part of the Agadir Melloul – Imoula inlier (**Fig. 3**), and the northern part of the Iguerda inlier (**Fig. 2C**). This monzogranite is characterized by: i) a porphyritic structure, resulting in the presence of abundant of K-feldspar phenocrysts; ii) its well-marked planar fabric; iii) the coexistence of two primary micas; and iv) the frequent presence of secondary white mica. The rare dark microgranular enclaves are rich in biotite, and with small size. The enclaves of metasedimentary rocks are of very variable size and distributed in a very irregular way.

Microscopic observation shows orthoclase tablets enchased in a matrix with medium grain (1 mm to 1 cm), hypidiomorphic and myrmekitic texture. The mineralogical composition is as follows: i) subhedral to euhedral, zoned plagioclase; ii) anhedral quartz, with abundant subgrains and strongly

undulating extinction; iii) orthoclase in two habitus: perthitic tablets, including small crystals of plagioclase and rare zoned quartz, and small anhedral crystals in matrix; iv) reddish brown biotite, frequently in the form of kinked lamellae, either isolated or in small clusters, and containing inclusions of zircon, rutile and rare apatite; and v) accessory minerals such as zircon, apatite, Fe-Ti oxides, pyrite.

Mesocratic medium-grained monzogranite outcrops in the southern part of the Tazeroualt massif (**Fig. 2B**), the south-eastern part of the Azaghar Izazen inlier (**Fig. 3**) and in the Zawyat-n-Dougadir massif (**Fig. 2C**). This mesocratic monzogranite is poor in primary muscovite and presents small dark biotite-rich, ovoid or flattened enclaves. Petrographic study of this monzogranite displays a medium-grained subhedral myrmekitic texture with the following mineralogical composition: i) subhedral to euhedral plagioclase, with frequent myrmekitic buds in contact with feldspar; ii) anhedral orthoclase, perthitic or not; iii) plates of anhedral quartz, interstitial with feldspars or in small rounded crystals corroding feldspar; iv) red brown biotite (7-10%) in slices usually grouped in small clusters; v) muscovite; and vi) zircon and apatite as accessory minerals.

The dark enclave has a fine-grained granoblastic texture with poikiloblastic muscovite. It is a hornfel consisting of the following minerals: i) polygonal plagioclase crystals (thermal annealing); ii) interstitial quartz; iii) abundant (20%) red-brown very fresh biotite in blastic flakes; iv) muscovite, in poikiloblastic plates; v) zircon and acicular apatite as accessories minerals.

3.4. Leucogranites

The leucocratic suite includes various types of granites: mesocratic to leucocratic, with two micas or muscovite alone and ends with pegmatites, locally very abundant. This suite is present in all the Paleoproterozoic inliers (**Figs. 2 and 3**). This association is represented by: i) a porphyritic two-mica granite; ii) a medium-grained two-mica leucogranite; iii) a medium- to coarse-grained two-mica leucogranite; iv) a medium-grained muscovite leucogranite; and v) fine to medium-grained muscovite-garnet leucogranite.

Porphyritic two-mica granite is heterogranular porphyritic granite with large K-feldspars, up to 10 cm locally. These K-feldspars consist of perthitic microcline in a matrix consisting of an assemblage of quartz, plagioclase, K-feldspar, more or less chloritized biotite and frequent muscovite. The abundance of microcline phenocrysts is not homogeneous. In some areas, especially in the

northwestern part of the Azaghar-Izazen inlier, these crystals are very abundant and large (length ≤8 cm), which gives to the rock an aspect of feldspar cumulate with a relatively light color, pale pink to white. In other areas, for example, their concentration is relatively low, while their planar orientation is very obvious.

Medium-grained two-mica leucogranite is homogeneous, with an equigranular texture, and heterogeneously deformed. It is distinguished from the others by increasing the percentage of biotite and the amounts of feldspar phenocrysts.

These leucogranites contain subhedral to euhedral plagioclase, showing polysynthetic twin planes frequently distorted, but generally little sericitized. K-feldspar is microcline in anhedral plates of variable size, the largest covering small crystals of plagioclase, quartz and altered biotite. It is often transformed into secondary white mica. Quartz consists of anhedral crystals, undulating to extinction, with abundant subgrains. Biotite is transformed into green chlorite + Fe-Ti minerals + sometimes a small amount of adularia and/or secondary white mica. Primary muscovite is frequently in kinked lamellae, scattered or in small clusters, associated with altered biotite. The secondary white micas are developed at the expense of feldspars and biotite. Accessory minerals are: oxides, zircon and apatite.

Sub-leucocratic to leucocratic medium to coarse-grained two-mica granite is characterized by large K-feldspar phenocrysts that can reach 3 cm in length, and the coexistence of two micas. Muscovite is more abundant than biotite, frequently chloritized, and is the only mica in the most leucocratic facies. Texture is more or less equigranular, but a clear planar fabric locally appears. It is heterogeneously deformed and turned into cataclasis. Accessory minerals are apatite, zircon and Fe oxides and/or Ti. The matrix includes the following minerals: i) plagioclase in anhedral to subhedral crystals, commonly zoned; ii) anhedral quartz with wavy extinction; iii) chloritized biotite; and iv) accessory minerals such as zircon, apatite and Fe-Ti oxides. K-feldspar tablets, 1 to 3 cm in length, *are* embedded in a medium-grained matrix enclosing two micas with an orientation underlying a strong planar fabric. K-feldspar is a microcline occurring in two habitus: (i) subhedral tablets and (ii) small anhedral crystals, singly or in small clusters in the matrix, which has an anhedral texture with heterogeneous grain.

Medium-grained muscovite leucogranite is characterized by its highly leucocratic character, the absence of biotite being visible to the naked eye. It is leucocratic granite, with medium grain, whose size is generally lower than 1 cm, and with an heterogeneous deformation. It is distinguishable by the

absence or the scarcity of large K-feldspar tablets. This gives it a granulometry much more homogeneous, with size grain ranging from 0.1 to 1 cm. It contains quartz, plagioclase, potassic feldspar, muscovite, very little altered biotite and sometimes garnet.

The standard sample (ASPC617) presents a subhedral texture with a monzonitic tendency and a heterogeneous grain size: 0.1 to 8 mm with an average of about 2 mm. The mineralogical composition is as follows: i) subautomorphic to automorphic plagioclase, little sericitized; ii) microcline in xenomorphic beaches of variable size, largest including partially or completely of small white mica and/or plagioclase crystals; iii) xenomorphic quartz; iv) large kinked muscovite; and apatite, zircon, Fe and/or Ti oxides.

Fine to medium-grained muscovite-garnet leucogranites occur as in small intrusions in the Azaghar-Izazen inlier, intrusive into two-mica granites; in the Agadir Melloul-Imoula inlier, three small plutons are intrusive in micaschists or in leucocratic muscovite granite. In the southernmost part of the Agadir Melloul inlier, such late leucogranites accur as dykes and small stocks within mesocratic biotite granite, and in small bodies intrusive into subleucocratic to mesocratic medium-grained two-mica granite in the southeastern part of the Azaghar-Izazen.

It is leucocratic muscovite-rich granite. With a fine-grained equigranular texture, the mineralogical composition of this granite is as follows: i) sericitized subhedral to euhedral plagioclase; ii) abundant anhedral microcline; iii) quartz with wavy extinction; iv) muscovite; v) garnet retromorphozed in phyllosilicates and opaque minerals, vi) cordierite, more or less rounded, completely transformed into white mica.

4. Structural geology

Before the Eburnean granites were emplaced, the Paleoproterozoic sedimentary rocks have been subjected to two syn-metamorphic deformation phases. The first, ductile folding, phase tilted the bedding to a vertical position; the second was mostly expressed as a regional dextral shearing. A second, widespread, folding phase with vertical axes, reorganized the pre-existing structures in a late- to post-Eburnean orogenic context. The trace of this second folding phase were intersected by a major network of gabbro veins. In the area, the Panafrican orogeny was probably restricted to simple wrench faulting.

4.1. Deformation prior to the Eburnean granitoids

These deformations have been recognized only in the Paleoproterozoic sediments intruded by late Eburnean granitoids in the Tagragra n' Daouizid and the Tagragra Ouhallal (**Fig. 2A**).

4.1.1. D1 DEFORMATION

The first deformation, D1, affecting stratification, is a syn-schistose folding induced verticalization of strata. In the Tagragra n' Daouizid, the downward folding is outlined by an axial-plane cleavage, sometimes penetrative, usually difficult to observe. Overprinting relationships between S1 and S1' generally hide the stratification. The isoclinal fold hinge (P1) is outlined by the lithological contrast between metamorphosed pelite and sandstone. The stratification, although transposed, is sometimes preserved on the flanks of the P1 folds.

The P1 folds are too sporadic to be able to attribute a general vergence to them or to know if they are part of a regional folding. Metric to multi-hectometric in size, they show sub-horizontal or low-dip axes. The S1 axial plane schistosity is sub-vertical or very steeply inclined to the north. These structures are undoubtedly intersected by the granitic intrusions.

S1 schistosity is naturally best expressed in metapelites. It is highlighted by the crystallization of fine white mica and chlorite flakes. In more clastic layers, the clasts are poorly deformed and molded by neoformed phyllites. In some sandstone levels with little cement, this schistosity is almost absent.

4.1.2. D1' DEFORMATION

D1' deformation is outlined by a penetrative S1' schistosity, which homogeneously affects the Paleoproterozoic metasediments. S1' is the most remarkable schistosity, the one that appears at first glance on the outcrop. It generally appears more penetrative than S1 and forms the main pattern of the rock.

S1' is subvertical like S1, but it is distinguished by the fact that it intersects folds P1. It systematically forms a very small angle with S1, deviating from it by a maximum of 25° counterclockwise, which gives it a general vergence towards the east.

The intersection lineation between S1 and S1' is therefore subvertical. This lineation outlines the direction of the P1' folds that seem to appear only at a decimetric to plurimetric scale. No larger P1' folds could be identified with certainty. The D1' deformation therefore does not appear to have

disturbed the overall geometry of the structures acquired during the P1 folding, even though it appears more ductile. The vergence of these sub-vertical folds suggests a dexterous sliding along the early anisotropic planes S0 and/or S1. It is not uncommon to observe that the D1' deformation generates strike-slip structures when S1 is favourably oriented.

S1' appears microscopically as a flow schistosity or sometimes as a very strong crenulation. In metapelites S1' is defined by phyllite planes with white mica and chlorite and more rarely green biotite. When clasts are present these minerals crystallize in the pressure shades. The clasts are moderately deformed in the schistosity plane and undergo little dynamic recrystallization.

4.2. Synchronous deformation of granite emplacement

In granitic plutons, foliation is often discrete but becomes more visible along the shear zones. It is often underlined by a mineral fabric, such as preferentially oriented large K-feldspar phenocrysts. This orientation is more visible in the porphyritic granitoids, or with lenticular enclave oriented along the foliation. The deformed granites present at the ductile shear zone are locally characterized by the presence of a foliation define by alternate layers of quartzo-feldspathic aggregate and mica, and presence of mica fish. Such highly deformed granites have been observed on the southeastern border of the Iguerda inlier, along a NNE SSW-SE striking shear zone.

4.3. Deformation subsequent to the Eburnean granitoids

D2 deformation is expressed by a folding P2, of kilometre scale, which is visible on aerial and satellite photographs. This folding is drawn by the trajectory of the S1 schistosity and by the transposed S0 in the flanks of the P1 folds (**Fig. 2A**). D2 represents the last major folding event recorded in the Eburnean basement.

P2 folds have a sub-vertical axial plane, NNE-SSW oriented, and have a vertical or steeply northward dipping axis. P2 folds have a "Z" shape in profile, and suggests, on a regional scale, a dextral sliding towards the NE. This deformation affects the quartz veins, which show mullion and/or rodding structures (Potherat et al., 1991).

P2 folds are particularly expressed on the eastern edge of the Tagragra n' Daouizid. There they form a vast antiform fold followed to the east by a synform with a submeridian axial plane. This folding is clearly posterior to the granitic intrusions because it affects an aplite vein belonging to the vein

procession. The S2 schistosity associated with the P2 folds shows a constant direction between N15° to N20° and is inclined 70 to 80° to the WNW. In the fold hinges S2 is predominant. The intersection with S1 and S1' produces a well-developed pencil structure. These folds are clearly intersected by the gabbro networks, which demonstrate the anteriority of this D2 deformation.

The geometry of the D2 deformation suggests a northward increasing deformation gradient. This gradient is in a S2 virgation: from N0° to N15°E in less deformed areas to N30° to 40°E in the more deformed northern end. D2 could be part of a regional dextral strike-slip fault that generated subvertical "Z" shaped folds. The disharmonic folding between the central part of the inlier (poorly folded) and its southern end (highly folded) could indicate the occurrence of a dextral ductile shear zone. In the Tagragra Ouhallal, at the SE edge of the plutons, P2 folding is much more attenuated, although S2 is also observed at the outcrop scale. This area resembles a sheltered zone during D2 deformation.

In conclusion, the D2 deformation suggests a SW-NE trending regional dextral strike-slip fault along the plutons that acted as a hard core: shear on their northern edge, folding on the western end, and sheltered zone on the SW edge.

4.4. Pan-African deformation

The Tazeroualt thrust is a northeast dipping thrust. This thrust consists in a band of mylonitic to ultramylonitic tonalitic orthogneiss, 100 to 500 m wide and dipping 25 to 40° to the southwest, so that the strength of the mylonite varies between 750 and 400 meters. Above this tonalitic orthogneiss band, the volcanic-sedimentary Anezi Group is a tectonic slice wedged between the mylonite and the mesocratic granite of the southern Tazeroualt massif. The slicing of the Anezi Group implies that the major Tazeroualt thrust is due to a phase of the Pan-African orogeny or was reactivated during this deformation.

The northern and southern ends of the Tagragra N-Daouizid inlier are crossed by late subvertical SW-NE fault corridors. These faults developed under brittle-ductile to brittle conditions and are characterized by the formation of tectonic breccias 1 to 2 meters thick. These faults show normal play, and brecciate the Paleoproterozoic basement and shift the basal breccias with basement fragments of the Ouarzazate Group by about ten meters before being overlained by the upper conglomerates of the

475 Ouarzazate Group. These faults are contemporary with the magmatism of the Ouarzazate Group. This
476 deformation is linked to the last tectonic phase of the Pan-African orogeny.

477 **5. Geochemistry**

478 Representative whole-rock major- and trace-element compositions of the four groups of Eburnean
479 plutonic rocks are illustrated in **Figs. 4–10**, and listed in Supplementary **Tables S1** and **S2**. The
480 detailed analytical methods are available in the Electronic Supplementary Material, together with the
481 whole dataset (Table S1).

482 **5.1. Diorites**

483 Chemical analyses of four samples of quartz-diorite reveal SiO_2 content ranging from 48.7 to
484 52.9 wt%, which are those of mafic to intermediate rocks, with high levels in $Fe_2O_3^t$ (8.3-9.2 wt%) and
485 especially in MgO (7.1-11.0 wt%). However, the content of TiO_2 is low (0.31-0.42 wt%; **Fig. 4**). These
486 rocks are also rich in CaO (6.4-7.8 wt%), and poor in K_2O (1.4-2.9 wt%) and Na_2O (1.4-2.6 wt%).
487 These quartz-diorites are metaluminous (A/CNK=0.78-1.05), magnesian and alkali-calcic to calc-
488 alkaline rocks with high Mg# (0.77–0.84) and variable K_2O/Na_2O ratios (from 0.5 to 2.1; **Fig. 5**). They
489 fall in the field of diorite in the diagram ANOR-Q' (**Fig. 6**).

490 REE patterns of quartz-diorites are homogeneous, characterized by slightly fractionated LREE
491 ($[La/Sm]_n$=2.7-3.4; $[La/Yb]_n$=6.3-7.2), slightly fractionated HREE ($[Gd/Yb]_n$=1.2-1.5), and no or slightly
492 positive Eu anomalies (**Fig. 7**). LREE and HREE contents are homogeneous (La=8.5-10.9 ppm;
493 Yb=0.9-1.2 ppm). HREE are ten-fold lower compared to chondrites. These rocks show low to
494 moderate concentrations in Rb (48–98 ppm), Cs (1.2-2.1 ppm), and Pb (4.7-14.0 ppm), as well as Ba
495 (367-570 ppm) and Sr (196-427 ppm). HFSE contents are in the same range than in tonalites-
496 trondhjemites (Th=1.0-1.9 ppm; U=0.66-1.37 ppm, Nb=1.9-2.4 ppm, Zr=101-173 ppm). Quartz-diorites
497 exhibit higher transition element contents than tonalites and trondhjemites (V=116-183 ppm; Cr=226-
498 598 ppm; Ni=25-57 ppm). Diorites have multi-element patterns characterized by negative Nb-Ta and
499 Ti anomalies and positive U, Pb and Sr anomalies (**Fig. 8**).

500 **5.2. Tonalites and trondhjemites**

501 Tonalites show moderate SiO_2 contents (58.8-60.9 wt%), with intermediate $Fe_2O_3^t$ (6.3-7.9 wt%), MgO
502 (2.9-3.2 wt%), CaO (4.8-5.7 wt%), Na_2O (2.7-3.0 wt%) and K_2O contents (2.3-2.8 wt%; **Fig. 4**). These

tonalites are metaluminous (A/CNK=0.96-1.05), magnesian, and calc-alkaline rocks with high Mg# (0.59–0.67) and K_2O/Na_2O ratios close to 1 (from 0.8 to 1.0; **Fig. 5**).

Trondhjemites show moderate SiO_2 contents (66.8-72.4 wt%), low CaO (1.9-2.6 wt%), MgO (0.3-0.5 wt%) and $Fe_2O_3^t$ contents (1.0-2.7 wt%), variable K_2O contents (1.4-3.5 wt%), and high Na_2O (4.7-5.5 wt%; **Fig. 4**. These trondhjemites are slightly peraluminous (A/CNK=1.11-1.17), magnesian to ferroan, and alkali-calcic to calc-alkaline rocks with restricted Mg# (0.38–0.52) and low K_2O/Na_2O ratios (from 0.3 to 0.7; **Fig. 5**).

REE patterns of tonalites are characterized by slightly fractionated LREE ($[La/Sm]_n$=1.9-3.7; $[La/Yb]_n$=3.7-11.0), slightly fractionated HREE ($[Gd/Yb]_n$=1.3-1.8), and with light negative Eu anomalies (**Fig. 7**). HREE are ten-fold higher compared to chondrites. These rocks display moderate concentrations in Rb (101–129 ppm), Cs (4.8–7.0 ppm), and Pb (9.9–10.9 ppm), as well as Ba (407–903 ppm) and Sr (286–385 ppm), and low concentrations in Th (2.4-5.1 ppm), U (1.1-1.8 ppm), Nb (6.5-11.3 ppm), and Zr (148-250 ppm). Transition element contents are low (V < 58 ppm; Cr < 119 ppm; Ni < 21 ppm). Tonalites have multi-element patterns characterized by negative Nb-Ta and Ti anomalies and positive U and Pb anomalies (**Fig. 8**).

REE patterns of trondhjemites are characterized by fractionated LREE ($[La/Sm]_n$=2.9-3.8; $[La/Yb]_n$=6.4-13.2), fractionated HREE ($[Gd/Yb]_n$=1.2-2.1), and no positive or negative Eu anomalies (**Fig. 7**). HREE are ten-fold lower compared to chondrites. These rocks display moderate concentrations in Rb (55–100 ppm), Cs (3.4-4.1 ppm), and Pb (9.8-11.8 ppm), as well as Ba (534-998 ppm) and Sr (546-726 ppm), low concentration in Th (0.7-2.9 ppm), U (0.54-1.13 ppm), Nb (1.5-7.1 ppm), and Zr (62-97 ppm). Transition element contents are low (V < 37 ppm; Cr < 25 ppm; Ni < 9 ppm). Trondhjemites have multi-element patterns characterized by significant negative Nb-Ta and Ti anomalies and positive U, Pb and Sr anomalies (**Fig. 8**).

5.3. Granodiorites and monzogranites

Granodiorites and monzogranites are characterized by high SiO_2 contents (64.4-71.1 wt%). They show variable concentrations of Al_2O_3 (13.9-16.6 wt%), CaO (1.2-3.9 wt%), $Fe_2O_3^t$ (1.8-5.1 wt%), MgO (0.5-2.6 wt%). Na_2O concentrations are fairly constant (2.7 to 4.9%), like K_2O (2.1-4.3 wt%). They fall in the field of granodiorite and monzogranite in the diagram ANOR-Q' (**Fig. 6**). These rocks are

metaluminous to peraluminous (A/CNK=1.02 to 1.40), magnesian and alkali-calcic to calc-alkaline with variable Mg# (45-73), and variable K_2O/Na_2O ratios (from 0.5 to 1.6; **Fig. 5**).

Granodiorites and monzogranites have higher LREE (19.2-125.6 ppm) and HREE contents (Yb=0.9-5.4 ppm) than diorites, tonalites and trondhjemites. Two groups can be distinguished according to their REE patterns. The first group corresponds to fractionated REE patterns ($[La/Sm]_n$=3.4-4.8; $[La/Yb]_n$=8.8-18.0; **Fig. 7**), with slightly fractionated HREE ($[Gd/Yb]_n$=1.6-2.1), HREE ten-fold higher compared to chondrites ($[Yb]_n$=7.1-31.8; **Fig. 7**), and light negative Eu anomalies. The second group corresponds to fractionated REE patterns ($[La/Sm]_n$=3.4-5.7; $[La/Yb]_n$=16.7-30.9; **Fig. 7**), with fractionated HREE ($[Gd/Yb]_n$=1.9-4.2), HREE lower than ten times chondrites ($[Yb]_n$=5.3-9.4; **Fig. 7**), and light negative Eu anomalies. Rb (72-209 ppm), Cs (1.3-7.0 ppm), and Pb concentrations (6.0-19.9 ppm) are generally higher than in tonalites-trondhjemites, while Ba concentrations are in the same range (386-1063 ppm) and Sr concentrations (42–331 ppm) are lower than in tonalites-trondhjemites. HFSE concentrations are also higher than in tonalites-trondhjemites (Th=6.1-14.9 ppm; U=1.1-4.6 ppm; Nb=5.9-34.9 ppm; Zr=63-563 ppm). Transitions elements are negatively correlated with SiO_2 (V=16-42 ppm; Cr=23-101 ppm; Ni=10-52 ppm). Calc-alkaline granitoids of Group 1 have multi-element patterns characterized by negative Nb-Ta and Ti anomalies and light positive U and Pb anomalies (**Fig. 8**), while granitoids of Group 2 have negative Ba-Sr, Nb-Ta and Ti anomalies and light positive U and Pb anomalies (**Fig. 8**).

5.4. Leucogranites

Leucogranites form a tight compositional cluster dispaying high SiO_2 contents (69.4-76.6 wt%), with high K_2O (3.5-5.8 wt%), and Na_2O contents (2.7-4.3 wt%), and low contents in $Fe_2O_3^t$ (0.7-2.6 wt%), MgO (0.13-1.25 wt%), CaO (0.18-1.0 wt%), and TiO_2 (0.03-0.29 wt%; **Fig. 4**). They fall in the field of alkaline granite and syenogranite in the diagram ANOR-Q' (**Fig. 6**). These leucogranites have very high K_2O/Na_2O ratios (≥0.9 and up to 2.1), peraluminous (A/CNK=1.07-1.34) and ferroan to magnesian signatures, alkali-calcic to calc-alkaline compositions and variable Mg# (0.05–0.28) ranging from 0.21 to 0.66 (**Fig. 5**).

Leucogranites display heterogeneous trace element compositions compared with the previous suites, and may be subdivided into three groups. The first group is characterized by fractionated REE patterns ($[La/Sm]_n$=1.8-4.2; $[La/Yb]_n$=5.8-62.4; **Fig. 9**), with fractionated HREE ($[Gd/Yb]_n$=1.9-10.3),

HREE ten-fold lower compared to chondrites ($[Yb]_n$=1.4-4.7; **Fig. 9**), and negative Eu anomalies. The second group is characterized by slightly fractionated REE patterns ($[La/Sm]_n$=1.9-3.9; $[La/Yb]_n$=2.5-17.2; **Fig. 9**), with flat HREE ($[Gd/Yb]_n$=0.9-2.5), HREE ten-fold higher compared to chondrites ($[Yb]_n$=2.9-21.8; **Fig. 9**), and negative Eu anomalies. The third group is characterized low REE contents, with flat REE patterns ($[La/Sm]_n$=0.9-1.7; $[La/Yb]_n$=1.4-4.3; **Fig. 9**), with flat HREE ($[Gd/Yb]_n$=0.7-2.2), HREE lower than eight times chondrites ($[Yb]_n$=1.6-7.5; **Fig. 9**), and negative Eu anomalies. Leucogranites are particularly rich in Rb (111-385 ppm), Cs (1.36-37.2 ppm), Th (0.3-22.2 ppm) and U (0.46-5.80 ppm) compared to any other plutonic rocks, while also being the poorest in Sr (11-110 ppm), Nb (0.3-12.3 ppm) and Zr (7-147 ppm). Ba (53-598 ppm) and Pb (7.2-41.0 ppm) concentrations are similar to suites. Leucogranites are poor in transition elements (V=1-24 ppm; Cr=7-42 ppm; Ni=5-14 ppm). Group 1 leucogranites have multi-element patterns characterized by negative Ba-Sr and Ti anomalies, without significative negative Nb-Ta anomalies, and positive U and Pb anomalies (**Fig. 10**), while Group 2 leucogranites have negative Ba-Sr and Ti anomalies, without significative negative Nb-Ta anomalies, and positive U and Pb anomalies (**Fig. 10**). Finally, Group 3 leucogranites have multi-element patterns characterized by negative Ba-Sr and Ti anomalies, and positive U and Pb anomalies (**Fig. 10**).

6. Geochronology

Fresh rocks from five different samples were grinded using a steel crusher to isolated zircon grain from the ground matter. The resulting powders were sieved in the range of 50–250 mm. Grains were separated first using heavy liquids, then using a magnetic separator. In situ microprobe SHRIMP II analyses were made at the Australian National University, Canberra (Australia). For each sample, about 30 grains were mounted in epoxy plugs, and polished for U and Pb isotopes to be analysed by the ion microprobe. Spot analyses were carried out on zircon grains with both instruments. To identify internal structure and morphology (core, rims, cracks and alteration), zircon grains were imaged by reflected light photomicrographs and scanning electron microscopy (SEM) to get cathodoluminescence.

The SHRIMP analyses were performed following the analytical procedure described by Claoué-Long et al. (1995) and Willliams (1998). The zircon standards used to calibrate the U–Pb ratio were the AS3

588 zircon from the Duluth gabbro (USA) for the Australian microprobe (1099.1 ± 0.5 Ma; Paces and Miller,
589 1993).

590 The analyses out of the [90–110%] concordance interval, calculated with 100 x ($^{207}Pb/^{235}U$
591 age)/($^{207}Pb/^{206}Pb$ age) for ages > 1 Ga (Meinhold et al., 2011) and 100 x ($^{206}Pb/^{238}U$ age)/ ($^{207}Pb/^{235}U$
592 age) for ages < 1 Ga, were rejected (Faure and Mensing, 2005 and Talavera et al., 2012)

593 Whatever analytical approach was used, all the uncertainty calculations were made at the 2σ level
594 (95% confidence limit) using the ISOPLOT/EX program (version 3.00) of Ludwig (2003). For ages
595 younger than 1000 Ma, the plotted data correspond to $^{206}Pb^*/^{238}U$ ages of the analyses involved in the
596 calculation of obtained ages in the Terra-Wasserburg Inverse Concordia diagram. For ages older than
597 1000 Ma, the plotted data correspond to the $^{207}Pb^*/^{206}Pb^*$ ages for concordant analysis or extrapolated
598 ages in case of Discordia mixing line. Results are listed in Supplementary **Table S3**.

599 **6.1. Diorites**

600 A quartz-monzodiorite sample (ASPC631) has been collected in the Iguerda inlier. Zircons of the
601 ASPC631 sample display euhedral crystals of medium size (about 200 microns), colorless or pink,
602 usually clear and sometimes elongated. Twelve isotopic analyses were carried out on twelve different
603 grains. They all show very little to no contribution of common Pb and with one exception they are all in
604 the concordant interval [90-110%] (**Fig. 11**). The calculated upper intercepts age, determined using
605 eleven analyses, is **2038 ± 4 Ma** with a MSWD at 0.75. This makes it the oldest plutonic intrusion in
606 the region of Agadir Melloul.

607 **6.2. Tonalites and trondhjemites**

608 A tonalite sample (GPC101) has been collected in the Kerdous inlier. Zircon crystals of the GPC101
609 sample are small (50-80 µm, with a maximum size of 150 µm), and limpid and clear. Thirteen analyses
610 were performed on twelve different grains. The calculated upper intercepts Age, calculated from nine
611 remaining analyses is **2106 ± 12 Ma**, with a MSWD of 1.04 (**Fig. 11**). This age is interpreted as that of
612 the tonalite crystallization. Two analyses (9.1 and 13.1) are perfectly consistent with significant
613 inheritances to 2183 ± 13 Ma and 2188 ± 6 Ma. These ages are close to the age obtained on a
614 trondjhemite in the Kerdous inlier (Anezi Map, BGS, 2001).

615 **6.3. Granodiorites and monzogranites**

A mesocratic monzogranite sample (AMPC278) has been collected in the Agadir-Melloul inlier. The zircon crystals of the AMPC278 sample are heterogeneous medium-sized (~100-250 µm), colorless or reddish. Eleven analyses were performed on 10 different grains. All analyses are practically concordant. The age calculated using the 8 more concordant analysis, gives an upper intercepts Age at **2035.7 ± 4.9 Ma** with a MSWD at 0.66 (**Fig. 11**). This zircon crystallization age is interpreted as concording with the granite emplacement.

A mesocratic porphyritic monzogranite sample (IGPC478) has been collected in the Iguerda inlier. Zircon crystals of the IGPC478 sample display quite heterogeneous size, with a length of 100 to 200 microns and a width of 20 to 100 microns. Some crystals are limpid and clear, while others are darker and colorful. They can be elongated and sometimes exhibit concentric zonation visible in cathode-luminescence. Twelve analyses were performed on twelve different grains. Analysed grains contain very little common Pb. Two analyses are perfectly consistent with inheritances to 2076 ± 8 Ma and 2140 ± 14 Ma. Ten remaining analyses give an upper intercept age of **2034 ± 5 Ma**, with a MSWD of 0.76 (**Fig. 11**). This age is interpreted as concording with the monzogranite crystallization.

6.4. Leucogranites

A two-mica leucogranite sample (ASAH642) has been sampled in the Iguerda inlier. Zircon crystals of the ASAH642 sample are small (~100 µm). They are sometimes lengthened, clear and limpid or coloured. For the SHRIMP dating of Canberra, Australia, twelve analyses were performed on twelve different grains. They all show very little or no contribution of common Pb and with one exception they are all concordant or subconcordant (**Fig. 11**). Two analyses are perfectly consistent with significant inheritances to 2087 ± 8 Ma and 2108 ± 8 Ma. The dating with SHRIMP gives an upper intercept age at **2037 ± 5 Ma** (**Fig. 11**), interpreted as concording with the leucogranite crystallization.

7. Discussion

7.1. Petrogenesis of the magmatic suites

Eburnean plutonic rocks show a petrographic diversity as they include intermediate to felsic rocks. The chemistry of tonalites and trondhjemites suggests the involvement of low-K and K-rich mantle-derived magmas (**Fig. 12**). The chemistry of diorites suggests the involvement of K-rich mantle-derived magmas (**Fig. 12**). Within felsic rocks, the calc-alkaline suite displays less fractionated felsic granites

644 (65-72 wt%) compared to the leucocratic suite (69-76 wt%). The dominant phase of the calc-alkaline
645 suite is a monzogranite as opposed to leucogranites of the leucocratic suite. The calc-alkaline
646 monzogranites trend between two endmembers in the ternary CaO – K_2O/Na_2O – $Al_2O_3/(FeO^t + MgO)$
647 diagram (Laurent et al., 2014; **Fig. 12**). This observation suggests a dual origin by: (i) involvement of
648 K-rich mantle-derived magmas (**Fig. 12**), either as a component of the source and/or via magma
649 mixing/mingling as suggested by the occurrence of intermediate calc-alkaline rocks as part of the
650 suite; and (ii) melting of sedimentary materials. As calc-alkaline monzogranites, leucogranites trend
651 between two endmembers in the ternary CaO – K_2O/Na_2O – $Al_2O_3/(FeO^t + MgO)$ diagram (Laurent et
652 al., 2014; **Fig. 12**). This characteristic suggests a dual origin by: (i) melting of tonalitic materials; and
653 (ii) melting of sedimentary materials.

654 In **Figure 13**, contemporaneous late Neoarchean diorites and granites can be classified into three
655 groups: i) metaluminous diorites, with high FeO^t+MgO contents(>10 wt%) and poor in HFSE, requiring
656 involvement of mantle-derived magmas; ii) calc-alkaline monzogranites, with low FeO^t+MgO contents
657 (<10 wt%), high Sr+Ba contents (> 700 ppm), and HFSE (Nb+Zr+Y) higher than 170 ppm, requiring
658 involvement of mantle-derived magmas and crustal-derived melts; iii) and leucogranites, with low
659 FeO^t+MgO contents (<10 wt%), low Sr+Ba contents (< 700 ppm), and HFSE (Nb+Zr+Y) lower than
660 170 ppm, resulting from melting of crustal lithologies.

661 In the diagrams Zr *vs.* $(Nb/Zr)_N$ (**Fig. 14**), diorites belong to the magmatism field of subduction zones,
662 which is compatible with the obvious orogenic signature of these rocks. These rocks would derive from
663 the differentiation of a calc-alkaline basaltic magma resulting from the melting of a metasomatic
664 mantle source. Calc-alkaline monzogranites form a cluster at the limit between the field of subduction-
665 related suites and the field of calc-alkaline and alkaline collision-related plutons (**Fig. 14**). The
666 distribution between the A and B fields could result from the variability of the crustal contaminant
667 nature: young, poor in incompatible elements for the rocks located in the field A, and old, rich in
668 incompatible elements for the rocks located in the field B. Leucocratic granites plot essentially in the
669 field D of peraluminous leucogranites (**Fig. 14**). This leucogranitic magmatism displays granites
670 characteristics of metasedimentary crustal origin, or at least, a supracrustal origin (Chappell and
671 White, 1974).

672 Ages from the diorites, calc-alkaline monzogranites and peraluminous leucocratic granites of the
673 Agadir-Melloul and Iguerda inliers are bracketed between 2040 and 2035 Ma (Orosirian), and suggest

674 an emplacement over a short interval of time for all the plutonic rocks. Similar ages (2032 - 2037 Ma)
675 have been observed on Paleoproterozoic granites from the Zenaga inlier (Thomas et al., 2002). Ages
676 from the calc-alkaline monzogranites and peraluminous leucocratic granites of the Tagragra d'Akka
677 and Tafeltast-Kerdous inliers are bracketed between 2049 and 2043 Ma (Orosirian; ages obtained on
678 different zircons by Pb evaporation and U–Pb SIMS methods; Gasquet et al, 2004), in a short interval
679 of time like in the Agadir-Melloul and Iguerda inliers. These age shows overlapping with zircon U–Pb
680 ages of Paleoproterozoic granites from Igherm, Kerdous, Tagragra de Tata and Bas Drâa inliers (Aït
681 Malek et al., 1998; Walsh et al., 2002; Barbey et al., 2004). All these geochronological datings suggest
682 emplacement over a short interval of time for these widespread Orosirian magmatic event.

683 Some ages at 2076 ± 8 Ma, 2100 Ma and 2140 ± 14 were obtained from inherited zircons found in
684 ASPC631 quartz-monzodiorite and ASAH642 leucogranite samples. Close ages at 2.07–2.17 Ga from
685 cores or inherited zircons ages were also obtained by Gasquet et al. (2004) in the Tagragra d'Akka
686 and Kerdous–Tafeltast inliers (western Anti-Atlas), and Thomas et al. (2002) in Zenaga inlier.
687 According to these authors, these ages may testify to an older Rhyacian magmatic event
688 contemporaneous with the volcanics (metatuffs interbedded in schists) that yielded a zircon age of
689 2072 Ma in the Tagragra de Tata inlier (Walsh et al., 2002). This Rhyacian magmatic event, observed
690 in the Kerdous inlier, corresponds to a tonalitic to trondhjemite magmatic event dated at 2106 ± 12 Ma.

691 The magma crystallization ages and geochemical compositions of the studied plutons suggest that
692 diorites and two granites types are produced from the same source components, but in systematically
693 different proportions with ongoing syn- to post-collisional setting. The diorites formed by the melting of
694 K-rich mantle-derived magmas. Calc-alkaline monzogranites formed by melting of K-rich mantle-
695 derived magmas with the involvement of sedimentary materials. Leucogranites formed by melting of
696 Paleoproterozoic crustal lithologies, with sedimentary and tonalitic components. No inherited Archean
697 component has been found in zircons from diorites or granites.

698 **7.2. The Eburnean Orogen of the West African Craton**

699 The West African Craton is composed of Archean cratonic blocks bounded by Paleoproterozoic
700 mobile belts which are Birimian accretionary-collisional orogenic system (ca. 2.27-1.96 Ga; Milési et
701 al., 1989; Feybesse and Milési, 1994; Ama-Salah et al., 1996; Gasquet et al., 2003; Baratoux et al.,
702 2011; Grenholm et al., 2019). The basement is primarily exposed in the Man-Leo and Reguibat

703 shields, and in the Kedougou-Kéniéba and Anti-Atlas inliers. Both the Reguibat and Man-Leo shields
704 are composed of an Archean block, which is tectonically juxtaposed with Birimian crust. The Birimian
705 crust is composed of supracrustal rocks characterized by mafic to felsic volcanic, volcano-
706 sedimentary, and siliciclastic successions, intruded by multiple generations of contemporaneous
707 plutonic suites. These Paleoproterozoic supracrustal and plutonic rocks have been affected by
708 polyphase deformation and metamorphism during the Eburnean Orogeny (ca. 2.16-2.05 Ga;
709 Feybesse and Milési, 1994; Gasquet et al., 2003; Peucat et al., 2005; Feybesse et al., 2006; Baratoux
710 et al., 2011; de Kock et al., 2012; Perrouty et al., 2012; Block et al., 2016a; Lebrun et al., 2016;
711 Masurel et al., 2017; Grenholm et al., 2019).

712 In northern section of the WAC (*n*WAC), Birimian crust is exposed in the larger Reguibat Shield as
713 well as in the smaller Anti-Atlas inliers. In the Reguibat shield, the Birimian domain is subdivided into
714 the western Yetti and eastern Eglab terranes. The western Yetti terrane is dominated by large granite
715 domains whereas supracrustal sequences are more widespread in the eastern Eglab terrane (Peucat
716 et al., 2005). The oldest Birimian ages record emplacement of volcanic and plutonic rocks at around
717 2.20 Ga. In the Eglab terrane, these are represented by gabbroic and granitic orthogneisses dated to
718 ca. 2210-2175 Ma (Peucat et al., 2005). In the Yetti terrane, a Sm-Nd isochron age of 2229 ± 49 Ma
719 (*n*=4, MSWD=1.18) has been obtained from basalts (Abouchami et al., 1990). After a gap of ca.
720 50 My, a new period of calc-alkalic to alkalic-calcic magmatism occurs between ca. 2120-2070 Ma,
721 and is characterized by emplacement of intrusives, volcanism and sedimentation recorded in both the
722 Yetti and Eglab terranes (Lahondère et al., 2003; Peucat et al., 2005; Schofield et al., 2006).

723 The Eglab massif exhibits an Eburnean evolution characterized by two major orogenic stages. The
724 first one corresponds mainly to 2.21–2.18 Ga magmatic activity forming a metamorphosed batholith
725 composed of various juvenile calc-alkaline orogenic suites, compatible with a mature island-arc setting
726 (Peucat et al., 2005). The second orogenic stage is characterized by active margin magmatic suites
727 emplaced and deformed at ca. 2.09 Ga. They are intruded by large volumes of high-K post-orogenic
728 magmas at ca. 2.07 Ga (Peucat et al., 2005). Like in the Eglab massif, two major orogenic stages
729 have been observed in the Birimian evolution of the Sfariat region (northern Mauritania, Lahondère et
730 al., 2003). The oldest Paleoproterozoic rocks (> 2.18 Ga) comprise with amphibolitic schist and
731 gneiss, chert, impure marble and locally serpentinized pyroxenite. The protoliths to the supracrustal
732 rocks indicate formation in an oceanic and/or intra-arc basin. Anatexis and sinistral transpression took

733 place between c. 2117 and 2064 Ma, and timing and kinematics of the Eburnean events are similar to
734 those for the Leo Shield (Schofield and Gillespie, 2007). The second stage is characterized by two
735 main magmatic suites. The plutonic rocks, which intruded the supracrustal rocks of the Tmeimichat
736 Group, are essentially diorites and peraluminous granites. The latter has yielded an age of
737 2118 ± 14 Ma (Lahondère et al., 2003). The Adam Esseder Igneous Complex comprises a voluminous
738 pink monzogranite with subordinate porphyritic, rapakivi-type monzogranite, granite and gabbro, which
739 has yielded an age of 2059 ± 4 Ma (Lahondère et al., 2003).

740 In southern section of the WAC (*s*WAC), the basement consists of Birimian crust accreted against an
741 Archean cratonic block, where the Birimian domain is composed of an assortment of supracrustal
742 successions and multiple suites of intrusives that have been affected by polyphase deformation and
743 metamorphism (e.g. Milesi et al., 1989; Feybesse and Milesi, 1994; Doumbia et al., 1998; Egal et al.,
744 2002; Pouclet et al., 2006; Baratoux et al., 2011; Block et al., 2016a). Prior to 2150 Ma, the intrusions
745 define a magmatic suite of gabbro-diorite-tonalite-granodiorite-granite, predominantly magnesian to
746 weakly ferroan, calc-alkalic and metaluminous to weakly peraluminous (Loh and Hirdes, 1999;
747 Gasquet et al., 2003; Pawlig et al., 2006; Baratoux et al., 2011; Tapsoba et al., 2013; Tshibubudze et
748 al., 2015; Block et al., 2016b). Like the volcanic rocks, the plutonic rocks have compositions
749 comparable to rocks found in association with modern subduction zones.

750 Following 2150 Ma, the intrusions are essentially monzonite to granite, high-K calc-alkaline with higher
751 K, Th and Rb contents (Liégeois et al., 1991; Hirdes et al., 1993; Doumbia et al., 1998; Gasquet et al.,
752 2003; Baratoux et al., 2011). There was also a shift towards more peraluminous compositions, marked
753 by the emplacement of Bt-Ms bearing granites in southeastern, central and northwestern Baoule
754 Mossi between ca. 2095–2075 Ma (Doumbia et al., 1998; Ouattara, 1998; Egal et al., 2002; Hirdes
755 and Davis, 2002; Gueye et al., 2008; Vidal et al., 2009; Petersson et al., 2016). The increased
756 diversity can be attributed to a maturation of the crust and lithosphere with a development of
757 increasingly contrasting source rocks, and further amplified by changing P-T-x conditions in the source
758 region of the melts (Grenholm et al., 2019).

759 **7.3. A regional geodynamic model for the Anti-Atlas**

760 In the western Anti-Atlas, the Eburnean basement is composed by highly deformed Paleoproterozoic
761 meta-sediments, intruded by two suites of Paleoproterozoic granitoids. The Paleoproterozoic meta-

762 sediments are the oldest known rocks. They are highly deformed, having undergone two Eburnean
763 phases of syn-metamorphic deformation: a first phase of folding and a second, less developed phase
764 in conjunction with regional dextral shearing. Locally, tectonic deformation related to the Pan-African
765 orogeny are observed. In the Kerdous inlier, a Pan-African thrust involved Eburnean basement and
766 the Ediacaran volcano-sedimentary Anezi Group. In the Tagragra n' Daouizid, late Pan-African
767 deformation is characterized by normal faults contemporary with the magmatism of the Ouarzazate
768 Group.

769 The Eburnean plutonic rocks are mainly divided into two distinct events, the first one with tonalitic to
770 trondhjemitic affinity and the second one with moderate to high-K calc-alkaline affinity. The first event,
771 located in northern Tazeroualt (Kerdous inlier), is characterized by tonalitic to trondhjemitic
772 assemblage indicating a subduction environment. The second event is more complex and can be
773 subdivided into 1) a calc-alkaline assemblage *sensu stricto,* comprising diorite and quartz diorite,
774 indicating magmatism of a mainly mantle origin, 2) a moderate to high-K calc-alkaline association
775 comprising granodiorite and monzogranite, indicating magmatism of mantle origin with the
776 involvement of a sedimentary component, and 3) peraluminous leucocratic calc-alkaline assemblage
777 comprising granite, indicating melting of supracrustal materials at relatively low pressure in a syn- to
778 post-collisional setting. This second event clearly shows the evolution of the geodynamic context of
779 the *n*WAC margin towards a collisional setting. This configuration clearly shares similarities with the
780 one observed in Eburnean granitoids of the Reguibat Rise, and of the southern WAC.

781 In the eastern part of Guinea, the Paleoproterozoic Baoulé-Mossi domain that rims the margin of the
782 Archean Kénéma-Man craton, is made up of a variety of late Eburnean granitoids (c. 2090-2070 Ma,
783 Egal et al., 2002). The granodiorite, monzogranite and biotite-granite of this plutonic belt present a
784 calc-alkaline and highly potassic nature. In the ternary CaO – K_2O/Na_2O –$Al_2O_3/(FeO^t + MgO)$ diagram
785 (Laurent et al., 2014) (**Fig. 15**), the chemistry of granodiorites suggests the involvement of low K to K-
786 rich mantle-derived magmas. The biotite granites trend between two endmembers: (i) melting of a
787 tonalitic component; and ii) involvement of K-rich mantle derived magmas (**Fig. 15**). Finally,
788 monzogranites trend between two endmembers: (i) melting of sediments; and ii) involvement of K-rich
789 mantle derived magmas (**Fig. 15**). The occurrence of peraluminous granite in the Siguiri basin, at the
790 northern extension of the plutonic belt, may suggest that the convergence here was associated with
791 the local melting of metasedimentary rocks in the deeper part of the basin (Egal et al., 2002). Egal et

al. (2002) interpret this late Eburnean plutonic belt as an active magin, along which strike-slip tectonism accommodated regional convergence towards the end of the Eburnean cycle.

In the Kédougou-Kéniaba inlier (KKI), available geochronological data indicate polycyclic magmatic activity that lasted from ca. 2210 to 2060 Ma. The first peak of magmatic activity led to the formation of the Sandikounda amphibolite-gneiss plutonic complex, the Badon granodiorite-granite complex, the Mako volcanic belt, and the Sandikounda layered plutonic complex between ca. 2210 and 2160 Ma (Hirdes and Davis, 2002; Dioh et al., 2006; Gueye et al., 2008; Treloar et al., 2014). The second manifestation of magmatism was associated with the emplacement of the Laminia-Kaourou plutonic complex, which intruded volcanic rocks of the Mako greenstone belt. The Laminia-Kaourou plutonic complex is composed of calc-alkaline plutons of granodiorite, tonalite and granite, and has been dated between 2138 ± 6 Ma and 2127 ± 6 Ma (Dia et al., 1997). The last peak of magmatic activity was associated with the emplacement of Eburnean granitoids between ca. 2080 and 2060 Ma (Dia et al., 1997; Hirdes and Davis, 2002; Gueye et al., 2007, 2008; Lambert-Smith et al., 2016).

In the ternary CaO – K_2O/Na_2O –$Al_2O_3/(FeO^t + MgO)$ diagram (Laurent et al., 2014) (**Fig. 15**), the late Eburnean granitoids of the KKI are composed of two main clusters, medium-K monzodiorite to granodiorite and K-rich calc-alkaline granites. The chemistry of medium-K monzodiorite to granodiorite suggests the involvement of K-rich mantle-derived magmas. The K-rich calc-alkaline granites fall in the field of tonalites, and define a trend suggesting between two endmembers: (i) melting of a tonalitic component; and ii) involvement of K-rich mantle derived magmas (**Fig. 15**). Masurel et al. (2017) interpret this late Eburnean granitoids as the products of a deep crustal or mantle-generated thermal event. Eglinger et al. (2017) proposed that late Eburnean magmas derived from partial melting of metasomatised lithospheric mantle between ca. 2100 and 2080 Ma.

In the Reguibat Rise, late Eburnean granitoids outcrop in the Eglab terrane and the Sfariat area. In the Eglab terrane, the second orogenic stage is composed by the Aftout magmatic suite, including medium-K calc-alkaline dioritoids, high-K calc-alkaline granitoids and peralkaline granitoids (Peucat et al., 2005). The chemistry of medium-K calc-alkaline dioritoids suggests the involvement of K-rich mantle-derived magmas (**Fig. 15**). The high-K calc-alkaline granitoids trend between two endmembers in the ternary CaO – K_2O/Na_2O – $Al_2O_3/(FeO^t + MgO)$ diagram (Laurent et al., 2014; **Fig. 15**). This observation suggests a dual origin by: (i) involvement of K-rich mantle-derived magmas (**Fig. 15**); and (ii) melting of crustal component with a tonalitic composition. Finally, peralkaline granitoids define a

homogeneous cluster at the limit between two fields, suggesting an origin by melting of tonalitic components and sedimentary materials (**Fig. 15**). In the Sfariat area, the second orogenic stage is composed by the Tmeimechatt and Adam Esseder magmatic suites, including high-K calc-alkaline granodiorites and high-K metaluminous to peraluminous granitoids (Peucat et al., 2005). High-K calc-alkaline granodiorites define a cluster at the limit between three fields, suggesting a complex origin by melting of tonalitic components and sedimentary materials, essentially, with a little involvement of K-rich mantle-derived magma (**Fig. 15**). High-K metaluminous to peraluminous granitoids define a trend suggesting between two endmembers: (i) melting of a tonalitic component; and ii) sedimentary materials (**Fig. 15**).

In northern and southern WAC, late Eburnean granitoids show a large petrographic and geochemical diversity as they include intermediate to felsic rocks. The two dominant phases are medium to high-K calc-alkaline granitoids and peralkaline to peraluminous granites, as opposed to dioritoids only form subordinate massifs. In *s*WAC, high-K calc-alkaline evolved granites result mainly from the melting of a crustal component with a tonalitic composition. By contrast, in *n*WAC, evolved granites are essentially peraluminous, with the involvement of sedimentary materials. As a result, the respective petrogenesis of late Eburnean granitoids from the Reguibat rise and the Anti-Atlas shares similarities with a significant mantle contribution and the important role played by sediment-derived melts for the most felsic compositions. As suggested by Mortaji et al. (2000), this late Eburnean magmatism takes place in thick sedimentary sequences in a back-arc geodynamic context in a transpressional regime.

8. Conclusions

Three major stages are recognized in the Paleoproterozoic crustal evolution of the western Anti-Atlas: the first one is Rhyacian, corresponding to the emplacement of a tonalitic batholith in the range of 2.095–2.12 Ga. A second orogenic phase occurred at ca. 2070 Ma, as shown by late Rhyacian volcano-sedimentary series (Zenaga-Iguerda Group). Finally, these sediments are intruded by large volumes of calc-alkaline diorites and granites, and peraluminous leucocratic granites interpreted as resulting from syn- to post-orogenic processes occurred at ca. 2.05 to 2.035 Ga.

Geochemical data indicate that the Rhyacian tonalites and trondhjemites form at convergent plate boundaries, where subduction is taking place (an island-arc arc or an active continental margin). The Orosirian plutonic rocks show a geochemical heterogeneity: (i) the chemical features of diorites

correspond to calc-alkaline M-type suites; (ii) granodiorites and granites are typical calc-alkaline I-type granitoids, and (iii) leucogranites, with peraluminous composition, reflect a crustal melting.

While the Rhyacian magmatic event indicates a subduction environment, the early Orosirian magmatic event is more complex, and the geochemical signatures imply involvement of mantellic magmas and crustal melting. As suggested by Mortaji et al. (2000), the early Orosirian magmatism takes place in thick sedimentary sequences in a back-arc geodynamic context in a transpressional regime.

Late Eburnean granitoids from the Reguibat rise (Peucat et al., 2005) and the Anti-Atlas shares similarities with a significant mantle contribution and the important role played by sediment-derived melts for the most felsic compositions. The Anti-Atlas Rhyacian and Orosirian plutonic rocks may correspond to the second orogenic stage observed the Eglab massif (Peucat et al., 2005), which is characterized by active margin magmatic suites emplaced prior 2.09 Ga, intruded by large volumes of high-K post- orogenic magmas younger than 2.07 Ga (Peucat et al., 2005).

To better understand tectonic setting of the Eburnean granites, further geochemical and geochronological investigations must be carried out on the granites of the Kerdous inlier. According to O'Connor et al. (2010), granitic suites were emplaced prior 2.15 Ga in the Kerdous inlier, however these ages are poorly constrained (2187 ± 33 Ma and 2263 ± 38 Ma, O'Connor et al., 2010). These older granites may correspond to the first orogenic stage recognized in the Eglab massif, which corresponds to 2.21-2.18 Ga calc-alkaline batholiths (Peucat et al., 2005).

Acknowledgments

Support for this work was provided by the Ministère de l'Energie, des Mines, de l'Eau et de l'Environnement, Direction du Développement Minier, Division du Patrimoine Géologique, Rabat, Morocco under contract 19-2008/DG under the Plan National de Cartographie Géologique (PNCG).

Credit Authorship contribution statement

Olivier Blein: Interpretation of chemical data and wrote the manuscript

Philippe Chèvremont: Contributed in the field work, sampling, and to the writing of the manuscript

Thierry Baudin: Contributed in the field work, sampling, and to the writing of the manuscript

Ahmid Hafid: Contributed in the field work, sampling, and to the writing of the manuscript

878 Hassan Admou: Contributed in the field work, sampling, and to the writing of the manuscript

879 Abderrahmane Soulaimani: Contributed in the field work, sampling, and to the writing of the
880 manuscript

881 Hassan Ouanaimi: Contributed in the field work and sampling

882 Mohamed Bouabdelli: Contributed in the field work and sampling

883 Dominique Gasquet: Contributed in the field work, sampling, and to the writing of the manuscript

884 Maxime Padel: Contributed to the calculation of SHRIMP U/Pb ages and to the writing of the
885 manuscript

886

887

References

Abati, J., Aghzer, A.M., Gerdes, A., Ennih, N., 2010. Detrital zircons of Neoproterozoic sequences of the Moroccan Anti-Atlas belt. Precambrian Res. 181(1-4), 115–128.

Abouchami, W., Boher, M., Michard, A., Albarede, F., 1990. A major 2.1 Ga event of mafic magmatism in West Africa: An early stage of crustal accretion. J. Geophys. Res. 95, 17605–17629. https://doi.org/10.1029/JB095iB11p17605

Admou, H., Hafid, A., Soulaimani, A., Simon, B., El Janati, M., Blein, O., Ouanaïmi, H., Baudin, T., Chèvremont, P., Abia, E.H., Bouabdelli, M., 2013. Carte géol. Maroc (1/50 000), feuille Assaragh. Notes et Mémoires Serv. Géol., Maroc, n°550.

Agard, J., 1952. Découverte d'une diorite orbiculaire dans les terrains précambriens de la région de Taïfst (Anti-Atlas). Notes et Mémoires du Service Géologique, 95, 161–1661.

Aït Lahna, A., Youbi, N., Tassinari, C.C.G., Basei, M.A.S., Ernst, R.E., Chaib, L., Barzouk, A., Mata, J., Gärtner, A., Admou, H., Boumehdi, M.A., Söderlund, U., Bensalah, M.K., Bodinier, J.L., Maacha, L., Bekker, A., 2020. Revised stratigraphic framework for the lower Anti-Atlas supergroup based on U-Pb geochronology of magmatic and detrital zircons (Zenaga and Bou Azzer-El Graara inliers, Anti-Atlas Belt, Morocco), J. Afr. Earth Sci. 171, 103946 https://doi.org/10.1016/j.jafrearsci.2020.103946.

Aït Malek, H., Gasquet, D., Bertrand, J. M., Leterrier J., 1998. Géochronologie U-Pb sur les granitoïdes éburnéens et panafricains dans les boutonnières protérozoïques d'Igherm, du Kerdous et du Bas Drâa (Anti-Atlas occidental, Maroc). Comptes Rendus de l'Académie des Sciences, Paris 327, 819–826. https://doi.org/10.1016/S1251-8050(99)80056-1

Alvaro, J.J., Clausen, S., El Albani, A., Chellai, E.H., 2005. Facies distribution of Lower Cambrian cryptic microbial and epibenthic archaeocyathan–microbial communities in the western Anti-Atlas, Morocco. Sedimentology, 53, 35–53. https://doi.org/10.1111/j.1365-3091.2005.00752.x

Alvaro, J.J., Macouin, M., Ezzouhairi, M., Charif, A., Ait Ayad, N., Ribeiro, M.L., Ader, M., 2008. Late Neoproterozoic Carbonate Productivity in a Rifting Context: the Adoudou Formation and its Associated Bimodal Volcanism Onlapping the Western Saghro Inlier, Morocco. Special Publications 2008, 297. Geological Society, London, pp. 285–302. https://doi.org/10.1144/SP297.14

917 Alvaro, J.J., 2020. Calibrating δ13C and δ18O chemostratigraphic correlations across Cambrian strata
918 of SW Europe and Morocco, West Gondwana. Stratigraphy & Timescale v. 5, Elsevier (ed.).
919 https://doi.org/10.1016/bs.sats.2020.08.003
920 Ama-Salah, I., Liégeois, J.-P., Pouclet, A., 1996. Evolution d'un arc insulaire océanique birimien
921 précoce au Liptako nigérien (Sirba) : géologie, géochronologie et géochimie. J. Afr. Earth Sci. 22,
922 235–254. https://doi.org/10.1016/0899-5362(96)00016-4
923 Baidada, B., Cousens, B., Alansari, A., Soulaimani, A., Barbey, P., Ilmen, S., Ikenne, M., 2017.
924 Geochemistry and Sm-Nd isotopic composition of the Imiter Pan-African granitoids (Saghro massif,
925 eastern Anti-Atlas, Morocco): Geotectonic implications. J. Afr. Earth Sci. 127, 99–112.
926 https://doi.org/10.1016/j.jafrearsci.2016.08.016
927 Baidada, B., Ikenne, M., Barbey, P., Soulaimani, A., Cousens, B., Haissen, F., Ilmen, S., Alansari, A.,
928 2019. SHRIMP U-Pb zircon geochronology of the granitoids of the Imiter inlier: Constraints on the
929 Pan-African events in the Saghro massif, Anti-Atlas (Morocco). J. Afr. Earth Sci. 150, 799–810.
930 https://doi.org/10.1016/j.jafrearsci.2018.10.008
931 Bajja, A., 1998. Volcanisme syn à post-orogénique du Néoprotérozoïque de l'Anti-Atlas: implications
932 pétrographiques et géodynamiques (Thèse de doctorat d'Etat). Université Chouaib Doukkali, El
933 Jadida, Maroc (215 p.).
934 Baratoux, L., Metelka, V., Naba, S., Jessell, M.W., Grégoire, M., Ganne, J., 2011. Juvenile
935 Paleoproterozoic crust evolution during the Eburnean orogeny (2.2-2.0 Ga), western Burkina Faso.
936 Precambrian Res. 191, 18–45. https://doi.org/10.1016/j.precamres.2011.08.010
937 Barbey, P., Oberli, F., Burg, J.P., Nachit, H., Pons, J., Meier, M., 2004. The Palaeoproterozoic in
938 western Anti-Atlas (Morocco): a clarification. J. Afr. Earth Sci. 39, 239–245.
939 Baudin, T., Razin, P., Chèvremont, P., Calvès, G., Gabudianu, D., Roger, J., 2005. Carte géol. Maroc
940 (1/50 000), feuille Awkarda. Notes et Mémoires Serv. Géol., Maroc, n°497.
941 Baudin, T., Blein, O., Chèvremont, Ph., Soulaimani, A., Ouanaimi, H., Roger, J., Admou, H., Hafid, A.,
942 Bouabdelli, M., Abia, E.H., 2013. Carte géol. Maroc (1/50 000°, feuille Tabadrist. Notes et
943 Mémoires Serv. Géol., Maroc, n°547.
944 Belkacim, S., Gasquet, D., Liégeois, J.P., Arai, S., Ghalan, H., Ahmed, H.A., Ishida, Y., Ikenne, M.,
945 2017. The Ediacaran volcanic rocks and associated mafic dykes of the Ouarzazate Group (Anti-
946 Atlas, Morocco): Clinopyroxene composition, whole-rock geochemistry and Sr-Nd isotopes

947 constraints from the Ouzellarh-Sirwa salient (Tifnoute valley). J. Afr. Earth Sci. 127, 113–135.
948 https://doi.org/10.1016/j.jafrearsci.2016.08.002
949 Benssaou, M., Hamoumi, N. 2001. L'Anti-Atlas occidental du Maroc: étude sédimentologique et
950 reconstitutions paléogéographiques au Cambrien inférieur. J. Afr. Earth Sci., 32, 351–372.
951 https://doi.org/10.1016/S0899-5362(01)90102-2
952 Benziane, F., 2007. Lithostratigraphie et évolution géodynamique de l'Anti-Atlas (Maroc) du
953 Paléoprotérozoïque au Néoprotérozoïque: exemples de la boutonnière de Tagragra de Tata et du
954 Jbel Saghro. PhD thesis. Université de Savoie CISM, Chambéry, France, 320 pp.
955 Benziane, F., Prost, A.E., Yazidi, A., 1983. Le passage du Précambrien au Cambrien précoce
956 volcanique et sédimentaire de l'Anti-Atlas; comparaisons avec l'Anti-Atlas occidental. Bulletin de la
957 Société géologique de France 25 (4): 549-556
958 BGS, 2001. Carte géologique de Tanalt au 1/50000. Notes et Mémoires, 401, Editions du Service
959 Géologiques du Maroc, Rabat.
960 Blein, O., Chèvremont, Ph., Baudin, T., Ouanaimi, H., Razin, Ph., Hafid, A., Admou, H., Soulaimani,
961 A., Bouabdelli, M, Abia, E.H., Beni Akhy, R., 2013. Notice explicative carte géol. Maroc (1/50 000),
962 feuille Tabadrist, Notes et Mémoires Serv. Géol. Maroc, n°547, MEM/BRGM. Carte géologique par
963 Baudin, T., Blein, O., Chèvremont, Ph., Soulaimani, A., Ouanaimi, H., Roger, J., Admou, H., Hafid,
964 A., Bouabdelli, M., Abia, E.H., 2013.
965 Blein, O., Baudin, T., Soulaimani, A., Cocherie, A., Chèvremont, Ph., Admou, H., Ouanaimi, H., Hafid,
966 A., Razin, Ph., Bouabdelli, M., Roger, J., 2014a. New Geochemical, Geochronological and
967 Structural Constraints on the Ediacaran Evolution of the South Sirwa, Agadir Melloul and Iguerda
968 Inliers, Anti-Atlas, Morocco. J. Afr. Earth Sci. 98, 47–71.
969 https://doi.org/10.1016/j.jafrearsci.2014.06.019
970 Blein, O., Baudin, T., Chèvremont, Ph., Soulaimani, A., Admou, H., Gasquet, D., Cocherie, A., Egal,
971 E., Youbi, N., Razin, Ph., Bouabdelli, M., Gombert, Ph., 2014b. Geochronological constraints on
972 the polycyclic magmatism in the Bou Azzer-El Graara inlier (Central Anti-Atlas Morocco). J. Afr.
973 Earth Sci. 99, 287–306. https://doi.org/10.1016/j.jafrearsci.2014.04.021
974 Block, S., Jessell, M., Aillères, L., Baratoux, L., Bruguier, O., Zeh, A., Bosch, D., Caby, R., Mensah,
975 E., 2016a. Lower crust exhumation during Paleoproterozoic (Eburnean) orogeny, NW Ghana, West

976 African Craton: interplay of coeval contractional deformation and extensional gravitational collapse.
977 Precambrian Res. 274, 82–109. https://doi.org/10.1016/j.precamres.2015.10.014
978 Block, S., Baratoux, L., Zeh, A., Laurent, O., Bruguier, O., Jessell, M., Ailleres, L., Sagna, R., Parra-
979 Avila, L.A., Bosch, D., 2016b. Paleoproterozoic juvenile crust formation and stabilisation in the
980 south-eastern West African Craton (Ghana); New insights from UPb-Hf zircon data and
981 geochemistry. Precambrian Res. 287, 1–30.
982 Bodinier, J.L., Dupuy, C., Dostal, J., 1984. Geochemistry of Precambrian ophiolites from Bou Azzer,
983 Morocco. Contrib. to Mineral. Petrol. 87, 43–50. https://doi.org/10.1007/BF00371401
984 Boudda, A., Choubert, G., Faure-Muret, A., 1979. Essai de stratigraphie de la couverture sédimentaire
985 de l'Anti-Atlas : Adoudounien-Cambrien inférieur. Notes et Mémoires du Service Géologique du
986 Maroc 271, 96 p.
987 Bouougri, E.H., Saquaque, A., 2004. Lithostratigraphic framework and correaltion of the
988 Neoproterozoic northern West African Craton passive margin sequence (Siroua – Zenaga - Bou
989 Azzer El Graara inliers, central Anti-Atlas, Morocco): an integrated approach. J. Afr. Earth Sci. 99,
990 287–306. https://doi.org/10.1016/j.jafrearsci.2004.07.045
991 Bouougri, E.H., Ait Lahna, A., Tassinari, C.C.G., Basei, M.A.S., Youbi, N., Admou, H., Saquaque, A.,
992 Boumedhi, M.A., Maacha, L., 2020. Time constraints on Early Tonian rifting and Cryogenian arc
993 terrane-continent convergence along the northern margin of the West African craton: Insights from
994 SHRIMP and LA-ICP-MS zircon geochronology in the Pan-African Anti-Atlas belt (Morocco).
995 Gondwana Res. 85, 169–188. https://doi.org/10.1016/j.gr.2020.03.011
996 Bousquet, R., El Mamoun, R., Saddiqi, O., Goffé, B., Möller, A., Madi, A., 2008. Mélanges and
997 ophiolites during the Pan-African orogeny: the case of the Bou-Azzer ophiolite suite (Morocco).
998 Geol. Soc. London, Spec. Publ. 297, 233–247. https://doi.org/10.1144/SP297.11
999 Calvès, G., Gabudianu, D., Chèvremont, P., Roger, J., Razin, P., 2005. Carte géol. Maroc (1/50 000),
1000 feuille Tlatat Ida Gougmar. Notes et Mémoires Serv. Géol., Maroc, n°498.
1001 Chappell, B.W., White, A.J.R., 1974. Two contrasting granite types. Pacific Geology 8, 173–174.
1002 Cheilletz, A., Levresse, G., Gasquet, D., Azizi Samir, M.R., Zyadi, R., Archibald, D.A., 2002. The Imiter
1003 epithermal deposit (Morocco): new petrographic, microtectonic and geochronological data.
1004 Importance of the Precambrian–Cambrian transition for Major precious metals deposits in the Anti-
1005 Atlas. Miner. Deposita 37, 772–781.

1006 Chèvremont, Ph., Blein, O., Razin, Ph., Simon, B., Baudin, T., Ouanaïmi, H., Soulaimani, A., El Janati,
1007 M., Bouabdelli, M., Abia, E.H., Admou, H., Hafid, A., Beni Akhy, R., 2013. Notice explicative carte
1008 géol. Maroc (1/50 000), feuille Ighriy, Notes et Mémoires Serv. Géol. Maroc, n°548, MEM/BRGM.
1009 Carte géologique par Ouanaimi, H., Chèvremont, Ph., Blein, O., Simon, B., Baudin, T., Razin, Ph.,
1010 Smektala, F., Soulaimani, A., El Janati, M., Abia, E.H., Admou, H., Hafid, A., Bouabdelli, M., 2013.
1011 Choubert, G., 1947. L'accident majeur de l'Anti-Atlas: Comptes Rendus de l'Académie des Sciences,
1012 Paris, 224,1172–1173.
1013 Choubert, G., 1952. Histoire géologique du domaine de l'Anti-Atlas. In: Géologie du Maroc. Notes et
1014 Mémoires du Service Géologique du Maroc 100, 75–194.
1015 Choubert, G., 1953a. Histoire géologique du domaine de l'Anti-Atlas. Notes et Mémoire de Service
1016 géologique du Maroc 100, 1–77.
1017 Choubert, G., 1953b. Le Précambrien III et le Géorgien de l'Anti-Atlas. Notes et Mémoire de Service
1018 géologique du Maroc 103, 7–39.
1019 Choubert, G., 1958. L'Adoudounien et le Précambrien de l'Anti-Atlas, in Les relations entre le
1020 Précambrien et le Cambrien. Colloque int. Centre National Recherche Scientifique, Colloque
1021 International, Paris 76, 143–162.
1022 Claoué-Long, J. C., Compston, W., Roberts, J., Fanning, C. M., 1995. Two Carboniferous ages: a
1023 comparison of SHRIMP zircon dating with conventional zircon ages and $^{40}Ar/^{39}Ar$ analysis.
1024 Geochronology Time Scales and Global Stratigraphic Correlation. SEPM Special Publication 54,
1025 1–21.
1026 Clauer, N., 1976. Géochimie isotopique du Strontium des milieux sédimentaires. Application à la
1027 géochronologie de la couverture du Craton Ouest-Africain. Strasbourg.
1028 Compston, W., Williams, I.S., Kirschvink, J.L., Zhang, Z., Ma, G., 1992. Zircon U/Pb ages for the early
1029 Cambrian timescale. Journal of the Geological Society of London, 149, 171–184.
1030 https://doi.org/10.1144/gsjgs.149.2.0171
1031 D'Lemos, R.S., Inglis, J.D., Samson, S.D., 2006. A newly discovered orogenic event in Morocco:
1032 Neoproterozic ages for supposed Eburnean basement of the Bou Azzer inlier, Anti-Atlas
1033 Mountains. Precambrian Res. 147, 65–78. https://doi.org/10.1016/j.precamres.2006.02.003.

1034 Decitre, S., Gasquet, D., Marignac, C., 2002. Genesis of orbicular granitic rocks from the Ploumanac'h
1035 Plutonic Complex (Brittany, France) petrographical, mineralogical and geochemical constraints.
1036 Eur. J. Mineral., 14, 715–731.
1037 De Kock, G.S., Théveniaut, H., Botha, P.M.W., Gyapong, W., 2012. Timing the structural events in the
1038 Paleoproterozoic Bolé-Nangodi belt terrane and adjacent Maluwe basin, West African craton, in
1039 central-west Ghana. J. Afr. Earth Sci. 65, 1–24. https://doi.org/10.1016/j.jafrearsci.2011.11.007
1040 Dia, A., Van Schmus, W.R., Kröner, A., 1997. Isotopic constraints on the age andformation of a
1041 Palaeoproterozoic volcanic arc complex in the Kédougou inlier, eastern Senegal, West Africa. J.
1042 Afr. Earth Sci. 24, 197–213.
1043 Diaz-Alvarado, J., Rodriguez, N., Rodriguez, C., Fernandez, C., Constanzo., I., 2017. Petrology and
1044 geochemistry of the orbicular granitoid of Caldera, northern Chile. Models and hypotheses on the
1045 formation of radial orbicular textures, Lithos, doi:10.1016/j.lithos.2017.04.017
1046 Dioh, E., Béziat, D., Debat, P., Grégoire, M., Ngom, P.M., 2006. Diversity of the Palaeoproterozoic
1047 granitoids of the Kédougou inlier (eastern Senegal): petrographicaland geochemical constraints. J.
1048 Afr. Earth Sci. 44, 351–371
1049 Doumbia, S., Pouclet, A., Kouamelan, A., Peucat, J.J., Vidal, M., Delor, C., 1998. Petrogenesis of
1050 juvenile-type Birimian (Paleoproterozoic) granitoids in central Cote d'Ivoire, West Africa:
1051 geochemistry and geochronology. Precambrian Res. 87, 33–63.
1052 Ducrot, J., Lancelot, J.R., 1977. Problème de la limite Précambrien-Cambrien : étude radio-
1053 chronologique par la méthode U-Pb sur zircons du volcan du Jbel Boho (Anti-Atlas Marocain).
1054 Canadian J. Earth Sci. 14, 2771–2777.
1055 Eddif, A., Gasquet, D., Hoepffner, Ch., Levresse, G., 2007. Age of the Wirgane granodiorite intrusions
1056 (Western High-Atlas, Morocco): new U-Pb constraints. J. Afr. Earth Sci., 47, 227–231.
1057 Egal, E., Thiéblemont, D., Lahondère, D., Guerrot, C., Costea, C.A., Iliescu, D., Delor, D., Goujou, J.-
1058 C., Lafon, J.M., Tegyey, M., Diaby, S., Kolie, P., 2002. Late Eburnean granitization and tectonics
1059 along the western and northwestern margin of the Archean Kenema-Man domain (Guinea, West
1060 African Craton). Precambrian Res. 117, 57–84.
1061 Eglinger, A., Thébaud, N., Zeh, A., Davis, J., Miller, J., Parra-Avila, L.A., Loucks, R., McCuaig, C.,
1062 2017. New insights into the crustal growth of the Paleoproterozoic margin of the Archean Kénéma-

1063 Man domain, West African Craton (Guinea): Implications for gold mineral system. Precambrian
1064 Res. 292, 258–289.
1065 El Baghdadi, M., El Boukhari, A., Jouider, A., Benyoucef, A., Nadem, S., 2003. Calc-alkaline arc I-type
1066 granitoid associated with S-type granite in the Pan-African belt of eastern Anti-Atlas (Saghro and
1067 Ougnat, South Morocco). Gondwana Res. 6 (4), 557–572. https://doi.org/10.1016/S1342-
1068 937X(05)71007-8
1069 El Bahat, A. Ikenne, M., Söderlund, U., Cousens, B., Youbi, N., Ernst, R., Soulaimani, A., El Janati,
1070 M., Hafid, A., 2013. U-Pb baddeleyite ages and geochemistry of dolerite dykes in the Bas Draa
1071 inlier of the Anti-Atlas of Morocco: newly identified 1380 Ma event in the West African Craton.
1072 Lithos. 174, 85–98. https://doi.org/10.1016/j.lithos.2012.07.022
1073 El Hadi, H., Simancas, J.F., Martínez-Poyatos, D., Azor, A., Tahiri, A., Montero, P., Fanning, C.M.,
1074 Bea, F., González-Lodeiro, F., 2010. Structural and geochronological constraints on the evolution
1075 of the Bou Azzer Neoproterozoic ophiolite (Anti-Atlas, Morocco). Precambrian Res. 182, 1–14.
1076 https://doi.org/10.1016/j.precamres.2010.06.011
1077 Ennih, N., Liégeois, J.P., 2001. The Moroccan Anti-Atlas: the West African craton passive margin with
1078 limited Pan-African activity. Implications for the northern limit of the craton. Precambrian Res. 112,
1079 289–302. https://doi.org/10.1016/S0301-9268(01)00195-4
1080 Ennih, N., Liégeois, J.P., 2008. The Boundaries of the West African Craton, with Special Reference to
1081 the Basement of the Moroccan Metacratonic Anti-Atlas Belt. Special Publications 2008, 297.
1082 Geological Society, London, 1-17. https://doi.org/10.1144/SP297.1
1083 Errami, E., Bonin, B., Laduron, D., Lasri, L., 2009. Petrology and geodynamic significance of the post-
1084 collisional Pan-African magmatism in the Eastern Saghro area (Anti-Atlas, Morocco). J. Afr. Earth
1085 Sci. 55, 105–124. https://doi.org/10.1016/j.jafrearsci.2009.02.006
1086 Errami, E., Linnemann, U., Hofmann, M., Gärtner, A., Zieger, J., Gärtner, J., Mende, K., El Kabouri, J.,
1087 Gasquet, D., Ennih, N., 2020. From Pan-African Transpression to Cadomian Transtension at the
1088 West African Margin: New U–Pb zircon Ages from the Eastern Saghro Inlier (Anti-Atlas, Morocco).
1089 *In* Murphy, J. B., Strachan, R. A. and Quesada, C. (eds). Pannotia to Pangaea: Neoproterozoic and
1090 Paleozoic Orogenic Cycles in the Circum-Atlantic Region. Geological Society, London, Special
1091 Publications, 503. https://doi.org/10.1144/SP503-2020-105

1092 Ezzouhairi, H., Ribeiro, M.L., Ait Ayad, N., Moreira, M.E., Charif, A., Ramos, J.M.F., de Oliveira,
1093 D.P.S., Coke, C., 2008. The Magmatic Evolution at the Moroccan Outboard of the West African
1094 Craton between the Late Neoproterozoic and the Early Palaeozoic. Special Publications 2008, 297.
1095 Geological Society, London, 329–343. https://doi.org/10.1144/SP297.16
1096 Faure, G., Mensing, T.M., 2005. Isotopes: principles and applications.Wiley, Hoboken (897 p.).
1097 Fekkak, A., Pouclet, A., Benharref, M., 2003. The Middle Neoproterozoic Sidi Flah Group (Anti-Atlas,
1098 Morocco): synrift deposition in a Pan- African continent/ocean transition zone. J. Afr. Earth Sci. 37,
1099 73–87. https://doi.org/10.1016/S0899-5362(03)00049-6
1100 Feybesse, J.L., Milési, J.-P., 1994. The Archean/Paleoproterozoic contact zone in West Africa: a
1101 mountain belt of décollement thrusting and folding on a continental margin related to 2.1 Ga
1102 convergence of Archean cratons? Precambrian Res. 69, 199–227. https://doi.org/10.1016/0301-
1103 9268(94)90087-6
1104 Feybesse, J.L., Billa, M., Guerrot, C., Duguey, E., Lescuyer, J.L., Milési, J.P., Bouchot, V., 2006. The
1105 Paleoproterozoic Ghanaian province: Geodynamic model and ore controls, including regional
1106 stress modeling. Precambrian Res. 149, 149–196. https://doi.org/10.1016/j.precamres.2006.06.003
1107 Frost, B.R., Barnes, C.G., Collins, W.J., Arculus, R.J., Ellis, D.J., Frost, C.D., 2001. A geochemical
1108 classification for granitic rocks. Journal of Petrology 42, 2033–2048.
1109 Gasquet, D., Roger, J., Chalot-Prat, F., Hassenforder, B., Baudin, T., Chèvremont, P., Razin, P.,
1110 Benlakhdim, A., Mortaji, A., Benssaou, M., 2001. Notice explicative carte géol. Maroc (1/50 000),
1111 feuille Tamazrar, Notes et Mémoires Serv. Géol. Maroc, n°415 bis, MEM/BRGM. Carte géologique
1112 par Roger, J., Gasquet, D., Baudin, T., Chalot-Prat, F., Hassenforder, B., Marquer, D.,
1113 Chèvremont, P., Berrahma, A., Destombes, J. Razin, P., Benlakhdim, M., 2001.
1114 Gasquet, D., Barbey, P., Adou, M., Paquette, J.L., 2003. Structure, Sr-Nd isotope geochemistry and
1115 zircon U-Pb geochronology of the granitoids of the Dabakala area (Cote d'Ivoire): evidence for a
1116 2.3 Ga crustal growth event in the Palaeoproterozoic of West Africa. Precambrian Res. 127, 329–
1117 354. https://doi.org/10.1016/S0301-9268(03)00209-2
1118 Gasquet, D., Chèvremont, P., Baudin, T., Chalot-Prat, F., Guerrot, C., Cocherie, A., Roger, J.,
1119 Hassenforder, B., Cheilletz, A., 2004. Polycyclic Magmatism in the Tagragra and Kerdous-
1120 Tafeltast inliers (Western Anti-Atlas, Morocco). J. Afr. Earth Sci. 39, 3/5, 267–276.

1121 Gasquet, D., Levresse, G., Cheilletz, A., Azizi-Samir, M.R., Mouttaqi, A., 2005. Contribution to a
1122 geodynamic reconstruction of the Anti-Atlas (Morocco) during Pan-African times with the
1123 emphasis on inversion tectonics and metallogenic activity at the Precambrian-Cambrian transition.
1124 Precambrian Res. 140, 157–182. https://doi.org/10.1016/j.precamres.2005.06.009
1125 Gasquet, D., Ennih, N., Liégeois, J-P., Soulaimani, A., Michard, A., 2008. The Panafrican belt. In:
1126 Michard A., Saddiqi O., Chalouan A., Frizon de Lamotte D. (Eds.), Continental Evolution: The
1127 Geology of Morocco. Structure, Stratigraphy, and Tectonics of the Africa-Atlantic-Mediterranean
1128 Triple Junction, Springer Verl., Berlin, Heidelberg, 33–64.
1129 Geyer, G., 1990. Proposal of formal lithostratigraphical units for the Terminal Proterozoic to early
1130 Middle Cambrian of southern Morocco. Newsl. Stratigr. 22 (2/3), 87–109.
1131 Grenholm, M., Jessell, M., Thébaud, N., 2019. A geodynamic model for the Paleoproterozoic (2.27-
1132 1.96 Ga) Birimian Orogen of the southern West African Craton – insights into an evolving
1133 accretionary-collisional orogenic system. Earth Sci. Rev. 192, 138–193.
1134 Gueye, M., Siegesmund, S., Wemmer, K., Pawlig, S., Drobe, M., Nolte, N., Layer, P., 2007. New
1135 evidence for an early Birimian evolution in the West African Craton: an example from the
1136 Kédougou-Kéniéba inlier, southeast Senegal. S. Afr. J. Geol.110, 511–534.
1137 Gueye, M., Ngom, P.M., Diene, M., Thiam, Y., Siegesmund, S., Wemmer, K., Pawlig, S., 2008.
1138 Intrusive rocks and tectono-metamorphic evolution of the Mako Paleoproterozoic belt (eastern
1139 Senegal, West Africa). J. Afr. Earth Sci. 50, 88–110.
1140 Hassenforder, B., 1987. La Tectonique Panafricaine et Varisque de l'Anti-Atlas dans le Massif du
1141 Kerdous (Maroc). Thèse de doctorat es-Sciences. Université de Strasbourg, p. 220.
1142 Hassenforder, B., Roger, J., Baudin, T., Chalot-Prat, F., Gasquet, D., Berrahma, A., Chèvremont, P.,
1143 Marquer, D., Razin, P., Benlakhdim, M., 2001. Carte géol. Maroc (1/50 000), feuille Sidi Bou'addi.
1144 Notes et Mémoires Serv. Géol. Maroc, n°414.
1145 Hawkins, M.P., Beddoe-Stephens, B., Gillespie, M.R., Loughlin, S., Barron, H.F., Barnes, R.P.,
1146 Powell, J.H., Waters, C.N., Williams, M., 2001. Carte géologique du Maroc au 1/50 000, feuille
1147 Tiwit. Notes et Mémoires du Service Géologique du Maroc 404.
1148 Hefferan, K.P., Admou, H., Karson, J.A., Saquaque, A., 2000. Anti-Atlas (Morocco) role in
1149 Neoproterozoic western Gondwana reconstruction. Precambrian Res. 103, 89–96.
1150 https://doi.org/10.1016/S0301-9268(00)00078-4

1151 Hirdes, W., Davis, D.W., 2002. U-Pb geochronology of Paleoproterozoic rocks in the southern part of
1152 the Kedougou-Kenieba Inlier, Senegal, West Africa: evidence for diachronous accretionary
1153 development of the Eburnean Province. Precambrian Res. 118, 83–99.
1154 Hirdes, W., Senger, R., Adjei, J., Efa, E., Loh, G., Tettey, A., 1993. Explanatory Notes for the
1155 Geological Map of Southwest Ghana 1:100000: Sheets Wiawso (0603D), Asafo (0603C), Kukuom
1156 (0603B), Goaso (0603A), Sunyani (0703D) and Berekum (0703C). Geologisches Jahrbuch Reihe
1157 B, Heft 83. (139 pp).
1158 Hodel, F., Triantafyllou, A., Berger, J., Macouin, M., Baele, J.-M., Mattielli, N., Monnier, C., Trindale,
1159 R.I.F., Ducea, M.N., Chatir, A., Ennih, N., Langlade, J., Poujol, M., 2020. The Morrocan Anti-Atlas
1160 ophiolite: Timing and melting processes in an intra-oceanic arc-back-arc environment. Gondwana
1161 Res. 86, 182–202. https://doi.org/10.1016/j.gr.2020.05.014
1162 Hollard, H., Choubert, G., Bronner, G., Marchand, J., Sougy, J., 1985. Carte géologique du Maroc,
1163 échelle: 1/1.000.000. Notes Mém. Serv. Géol. Maroc, n°260.
1164 Ikenne, M., 1997. La Boutonnière précambrienne du Bas Drâa (Anti-Atlas occidental, Maroc):
1165 Caractérisation pétrologique et géochimique des roches magmatiques et métamorphiques et leurs
1166 relations avec la déformation. IbnZohr University, p. 256.
1167 Ikenne, M., Soderlund, U., Ernst, R., Pin, C., Youbi, N., El Aouli, E.H., 2017. A c. 1710 Ma mafic sill
1168 emplaced into a quartzite and calcareous series from Igherm, Anti-Atlas, Morocco: evidence that
1169 the Taghdout passive margin sedimentary group is nearly 1 Ga older than previously thought. J.
1170 Afr. Earth Sci. 127, 113–135. https://doi.org/10.1016/j.jafrearsci.2016.08.020
1171 Inglis, J.D., D'Lemos, R.S., Samson, S.D., Admou, H., 2005. Geochronological constraints on Late
1172 Precambrian intrusion, metamorphism, and tectonism in the Anti-Atlas Mountains. J. Geol. 113,
1173 439–450. https://doi.org/10.1086/430242
1174 Kouyaté, D., Söderlund, U., Youbi, N., Ernst, R., Hafid, A., Ikenne, M., Soulaimani, A., Bertrand, H., El
1175 Janati, M., R'kha Chaham, K., 2013. U-Pb baddeleyite and zircon ages of 2040 Ma, 1650 Ma and
1176 885 Ma on dolerites in the West African Craton (Anti-Atlas inliers): Possible links to break-up of
1177 Precambrian supercontinents. Lithos 174, 71–84. https://doi.org/10.1016/j.lithos.2012.04.028
1178 Lahondère, D., Thiéblemont, D., Goujou, J.-C., Roger, J., Moussine-Pouchkine, A., LeMetour, J.,
1179 Cocherie, A., Guerrot, C., 2003. Notice explicative des cartes géologiques et gitologiques à

1180 1/200 000 et 1/500 000 du Nord de la Mauritanie. vol. 1 DMG, Ministère des Mines et de l'Industrie,
1181 Nouakchott.
1182 Lambert-Smith, J.S., Lawrence, D.M., Müller, W., Treloar, P.J., 2016. Palaeotectonic setting of the
1183 south-eastern Kédougou-Kéniéba Inlier, West Africa: New insights from igneous trace element
1184 geochemistry and U-Pb zircon ages. Precambrian Res. 274, 110–135.
1185 http://dx.doi.org/10.1016/j.precamres.2015.10.013
1186 Landing, E., Bowring, S.A., Davidek, K.L., Westrop, S.R., Geyer, G., Heldmaier, W., 1998. Duration of
1187 the Early Cambrian: U–Pb ages of volcanic ashes from Avalon and Gondwana. Can. J. Earth Sci.
1188 35, 329–338.
1189 Laurent, O., Martin, H., Moyen, J.-F., Doucelance, R., 2014. The diversity and evolution of late-
1190 Archean granitoids: Evidence for the onset of “modern-style” plate tectonics between 3.0 and 2.5
1191 Ga. Lithos 205, 208–235. https://doi.org/10.1016/j.lithos.2014.06.012
1192 Leblanc, M., 1975. Ophiolites précambriennes et gites arséniés de Cobalt (Bou Azzer - Maroc).
1193 Université Paris VI, Paris.
1194 Lebrun, E., Thébaud, N., Miller, J., Ulrich, S., Bourget, J., Terblanche, O., 2016. Geochronology and
1195 lithostrathigraphy of the Siguiri district: Implications for gold mineralisation in the Siguiri Basin
1196 (Guinea, West Africa). Precambrian Res. 274, 136–160.
1197 Letsch, D., 2018. The Anti-Atlas Belt (Morocco) During the Proterozoic - A Sedimentary Perspective
1198 (Dissertation ETH n° 25216, Zurich, 201 p.).
1199 Leveson D.J. (1966): Orbicular rocks: a review. Geol. Soc. Am. Bull. 77,409-426.
1200 Liégeois, J.P., Claessens, W., Camara, D., Klerkx, J., 1991. Short-lived Eburnian orogeny in southern
1201 Mali. Geology, tectonics, U-Pb and Rb-Sr geochronology. Precambrian Res. 50, 111–136.
1202 Loh, G., Hirdes, W., 1999. Explanatory notes for the geological map of southwest Ghana 1:100000,
1203 Sekondi (0402A) and Axim (0403B) sheets. Geologisches Jahrbuch Reihe B, Heft 93. BGR,
1204 Hannover.
1205 Ludwig, K.R., 2003. Isoplot/Ex Version 3.00, A Geochronological Toolkit for Microsoft Excel: Berkeley
1206 Geochronology Center Special Publication 4, 73 pp.
1207 Maloof, A.C., Schrag, D.P., Crowley, J.L., Bowring, S.A., 2005. An expanded record of Early Cambrian
1208 carbon cycling for the Anti-Atlas margin, Morocco. Canadian. J. Earth Sci. 42, 2195–2216.
1209 https://doi.org/10.1139/e05-062

1210 Masurel, Q., Thébaud, N., Miller, J., Ulrich, S., 2017. The tectono-magmatic framework to gold
1211 mineralisation in the Sadiola-Yatela gold camp and implications for the paleotectonic setting of the
1212 Kédougou-Kénieba inlier, West Africa. Precambrian Res. 292, 35–56.
1213 McDonough, W.F., Sun, S.S., 1995. The composition of the Earth. Chem. Geol. 120 (3–4), 223–253.
1214 https://doi.org/10.1016/0009-2541(94)00140-4
1215 Meinhold, G., Morton, A.C., Fanning, C.M., Frei, D., Howard, J.P., Phillips, R.J., Strogen, D., Whitham,
1216 A.G., 2011. Evidence from detrital zircons for recycling of Mesoproterozoic and Neoproterozoic
1217 crust recorded in Paleozoic and Mesozoic sandstones of southern Libya. Earth Planet. Sci. Lett.
1218 312, 164–175. https://doi.org/10.1016/j.epsl.2011.09.056
1219 Michard, A., Soulaimani, A., Ouanaimiv, H., Raddi, Y., Ait Brahim, L., Rjimati, E., Baidder, L., Saddiqi,
1220 O., 2017. Saghro Group in the Ougnat Massif (Morocco), an evidence for a continuous Cadomian
1221 basin along the northern West African Craton. C. R. Geoscience 349, 81–90.
1222 https://doi.org/10.1016/j.crte.2017.01.001
1223 Milési, J.P., Feybesse, J.L., Ledru, P., Dommanget, A., Ouedraogo, M.F., Tegyey, M., Calvez, J.Y.,
1224 Lagny, P., 1989. Les minéralisations aurifères de l'Afrique de l'Ouest; leur évolution lithostructurale
1225 au Protérozoïque inférieur. Chronique de la Recherche Minière 497, 3–98.
1226 Mortaji, A., Ikenne, M., Gasquet, D., Barbey, P., Stussi, J.M., 2000. Les granitoïdes
1227 paléoprotérozoïques des boutonnières du Bas Drâa et de la Tagragra d'Akka (Anti-Atlas
1228 occidental, Maroc): un élément du puzzle géodynamique du craton ouest-africain. J. Afr. Earth Sci.
1229 31, 523–538. https://doi.org/10.1016/S0899-5362(00)80005-6
1230 O'Connor, E.A., Barnes, R.P., Beddoe-Stephens, B., Fletcher, T., Gillespie, M.R., Hawkins, M.P.,
1231 Loughlin, S.C., Smith, M., Smith, R.A., Waters, C.N., Williams, M., 2010. Geology of the Drâa,
1232 Kerdous, and Boumalne Districts, Anti-atlas, Morocco. Keyworth. Nottingham British Geological
1233 Survey, 324 p.
1234 Ouanaïmi, H., Chèvremont, P., Blein, O., Simon, B., Baudin, T., Razin, P., Smektala, F., Soulaimani,
1235 A., El Janati, M., Abia, E.H., Admou, H., Hafid, A., Bouabdelli, M., 2013. Carte géol. Maroc (1/50
1236 000), feuille Ighriy. Notes et Mémoires Serv. Géol., Maroc, n°548.
1237 Ouattara, G., 1998. Structure du batholite de Ferkessedougou (secteur de Zuenoula, Cote d'Ivoire).
1238 Université d'Orléans, ISTO, Orléans (Thèse doctorat, 291 pp).

1239 Ouguir, H., Macaudière, J., Dagallier, G., 1996. Le Protérozoïque supérieur d'Imiter, Saghro oriental,
1240 Maroc : un contexte géodynamique d'arrière-arc. J. Afr. Earth Sci. 22, 173–189.
1241 Paces, J.B., Miller, J.D., 1993. Precise U–Pb ages of Duluth Complex and related mafic intrusions,
1242 Northern Minnesota: geochronological insight to physical, petrogenic, and tectonomagmatic
1243 processes associated with the 1.1 Ga midcontinent rift system. J. Geophys. Res. 98, 13997–
1244 14013. https://doi.org/10.1029/93JB01159
1245 Pawlig, S., Gueye, M., Klischies, R., Schwarz, S., Wemmer, K., Siegesmund, S., 2006. Geochemical
1246 and Sr-Nd isotopic data on the Birimian of the Kedougou-Kenieba Inlier (eastern Senegal):
1247 Implications on the Palaeoproterozoic evolution of the West African Craton. S. Afr. J. Geol. 109,
1248 411–427.
1249 Perrouty, S., Aillères, L., Jessell, M.W., Baratoux, L., Bourassa, Y., Crawford, B., 2012. Revised
1250 Eburnean geodynamic evolution of the gold-rich southern Ashanti belt, Ghana, with new field and
1251 geophysical evidence of pre-Tarkwaian deformations. Precambrian Res. 204-205, 12–39.
1252 https://doi.org/10.1016/j.precamres.2012.01.003
1253 Petersson, A., Schersten, A., Kemp, A.I.S., Kristinsdottir, B., Kalvig, P., Anum, S., 2016. Zircon U-Pb-
1254 Hf evidence for subduction related crustal growth and reworking of Archaean crust within the
1255 Palaeproterozoic Birimian terrane, West African Craton, SE Ghana. Precambrian Res. 275, 286–
1256 309.
1257 Peucat, J.-J., Capdevila, R., Drareni, A., Mahdjoub, Y., Kahoui, M., 2005. The Eglab massif in the
1258 West African Craton (Algeria), an original segment of Eburnean orogenic belt: Petrology,
1259 geochemistry and geochronology. Precambrian Res. 136, 309–352.
1260 Piqué, A., Bouabdelli, M., Soulaïmani, A., Youbi, N., Iliani, M., 1999. Les conglomérats du PIII
1261 (Néoprotérozoïque supérieur) de l'Anti-Atlas (Sud du Maroc : molasses panafricaines ou
1262 marqueurs d'un rifting fini-protérozoïque ?). Comptes Rendus de l'Académie des Sciences, Paris
1263 328, 409-414.
1264 Potherat, P., Aït Kassi, M., Nicot, P., Macaudière, J., Marignac, C., 1991. Structural evolution of gold-
1265 bearing quartz veins in the Paleoproterozoic exposures of the Tagragra d'Akka (western Anti-Atlas,
1266 Morocco). Source, transport and deposition of metals, Pagel and Leroy (ed.). Balkerma,
1267 Rotterdam, 477–480.

1268 Pouclet, A., Doumbia, S., Vidal, M., 2006. Geodynamic setting of the Birimian volcanism in Central
1269 Cote d'Ivoire (western Africa) and its place in the Palaeoproterozoic evolution of the man shield.
1270 Bull. Soc. Geol. Fr. 177, 105–121.
1271 Roger, J., Gasquet, D., Baudin, T., Chalot-Prat, F., Hassenforder, B., Marquer, D., Chèvremont, P.,
1272 Berrahma, A., Destombes, J. Razin, P., Benlakhdim, M., 2001. Carte géol. Maroc (1/50 000),
1273 feuille Tamazrar. Notes et Mémoires Serv. Géol. Maroc, n°415.
1274 Saquaque, A., Admou, H., Cissé, A., Benyoussef, A., Reuber, I., 1989. Les intrusions calco-alcalines
1275 de la boutonnière de Bou-Azzer El Graara (Anti-Atlas): marqueurs de la déformation panafricaine
1276 majeure dans un contexte de collision d'arc. Comptes Rendues Académie des Sciences Paris.
1277 308, 1279–1283.
1278 Saquaque, A., Benharref, M., H., Abia, H., Mrini, Z., Reuber, I., Karson, J.A., 1992. Evidence for a
1279 Panafrican volcanic arc and wrench fault tectonics in the Jbel Saghro, Anti-Atlas, Morocco.
1280 Geologische Rundschau. 81 (1), 1–13.
1281 Schofield, D.I., Gillespie, M.R., 2007. A tectonic interpretation of "Eburnean terrane" outliers in the
1282 Reguibat Shield, Mauritania. J. Afr. Earth Sci. 49, 179–186
1283 Schofield, D.I., Horstwood, M.S.A., Pitfield, P.E.J., Crowley, Q.G., Wilkinson, A.F., Sidaty, H.Ch.O.,
1284 2006. Timing and kinematics of Eburnean tectonics in the central Reguibat Shield, Mauritania. J.
1285 Geo. Sci. 163, 549–560. https://doi.org/10.1144/0016-764905-097
1286 Soulaimani, A., Bouabdelli, M., Piqué, A., 2003. L'extension continentale au Néo-Protérozoïque
1287 supérieur-Cambrien inférieur dans l'Anti-Atlas (Maroc). Bulletin de la Société Géologique de
1288 France 174, 83-92.
1289 Soulaimani, A., Jaffal, M., Maacha, L., Kchikach, A., Najine, A., Saidi, A., 2006. Modélisation
1290 magnétique de la suture ophiolitique de Bon Azzer-El Graara (Anti-Atlas central, Maroc).
1291 Implications sur la reconstitution géodynamique panafricaine. C. R. Geoscience. 338, 153–160.
1292 Soulaimani, A., Blein, O., Chèvremont, Ph., Ouanaimi, H., Hafid, A., Admou, H., Baudin, T.,
1293 Bouabdelli, M, Razin, Ph., Abia, E.H., Beni Akhy, R., 2013. Notice explicative carte géol. Maroc
1294 (1/50 000), feuille Agadir Melloul, Notes et Mémoires Serv. Géol. Maroc, n°549, MEM/BRGM.
1295 Carte géologique par Blein, O., Roger, J., Chèvremont, Ph., Baudin, T., Soulaimani, A., Ouanaimi,
1296 H., Admou, H., Hafid, A., Abia, E.H., Bouabdelli, M., 2013.

1297 Soulaimani, A., Ouanaimi, H., Saddiqi, O., Baidder, L., Michard, A., 2018. The Anti-Atlas Pan-African
1298 Belt (Morocco): Overview and pending questions. C. R. Geoscience 350, 279–288.
1299 https://doi.org/10.1016/j.crte.2018.07.002
1300 Soulaimani, A., Ouanaimi, H., Michard, A., Monterod, P., Bead, F., Corsinie, M., Molinad, J.-F.,
1301 Rjimatif, E.C., Saddiqig, O., Hefferan, K. 2019. Quartzite crests in Paleoproterozoic granites (Anti-
1302 Atlas, Morocco); a hint to Pan-African deformation of the West African Craton margin. J. Afr. Earth
1303 Sci. 2019; 157(February):103501. doi:10.1016/j.jafrearsci.2019.05.009
1304 Streckeisen, A., Le Maitre, R.W., 1979. A chemical approximation to the modal QAPF classification of
1305 the igneous rocks. Neues Jahrbuch für Mineralogie, Abhandlungen 136, 169–206.
1306 Talavera, C., Montero, P., Martinez Poyatos, D., Williams, I.S., 2012.Ediacaran to Lower Ordovician
1307 age for rocks ascribed to the Schist-Graywacke Complex (Iberian Massif, Spain): evidence from
1308 detritalzircon SHRIMP U–Pb geochronology. Gondwana Res. 22, 928–942.
1309 https://doi.org/10.1016/j.gr.2012.03.008
1310 Tapsoba, B., Lo, C.-H., Jahn, B.-M., Chung, S.-L., Wenmenga, U., Iizuka, Y., 2013. Chemical and Sr-
1311 Nd isotopic compositions and zircon U-Pb ages of the Birimian granitoids from NE Burkina Faso,
1312 West African Craton: Implications on the geodynamic setting and crustal evolution. Precambrian
1313 Res. 224, 364–396.
1314 Thiéblemont, D., Tegyey, M., 1994. Une discrimination géochimique des roches différenciées témoin
1315 de la diversité d'origine et de situation tectonique des magmas calco-alcalins. C. R. Acad. Sci.
1316 Paris 319 (série II), 87–94.
1317 Thomas, R.J., Chevallier, L.C., Gresse, P.G., Harmer, R.E., Eglington, B.M., Armstrong, R.A., de
1318 Beer, C.H., Martini, J.E.J., de Kock, G.S., Macey, P., Ingram, B., 2002. Precambrian evolution of
1319 the Siroua Window, Anti-Atlas Orogen, Morocco. Precambrian Res. 118, 1-57.
1320 https://doi.org/10.1016/S0301-9268(02)00075-X
1321 Thomas, R.J., Fekkak, A., Ennih, N., Errami, E., Loughlin, S.C., Gresse, P.G., Chevallier, L.P.,
1322 Liégeois, J.-P., 2004. A new lithostratigraphic framework for the Anti-Atlas Orogen, Morocco. J. Afr.
1323 Earth Sci. 39, 217–226. https://doi.org/10.1016/j.jafrearsci.2004.07.046
1324 Toummite, A., Liégeois, J.-P., Gasquet, D., Bruguier, O., Beraaouz, E.H., Ikenne, M., 2012. Field,
1325 geochemistry and Sr-Nd isotopes of the Pan- African granitoids from the Tifnoute Valley (Sirwa,

Anti-Atlas, Morocco): a post-collisional event in a metacratonic setting. Mineral. Petrol. 107 (5), 739–763. https://doi.org/10.1007/s00710-012-0245-3

Treloar, P.J., Lawrence, D.M., Senghor, D., Boyce, A., Harbidge, P., 2014. The Massawa gold deposit, Eastern Senegal, West Africa: an orogenic gold deposit sourced from magmatically derived fluids? Geol. Soc. Lond. Spec. Publ. 393, SP393–SP412.

Triantafyllou, A., Berger, J., Baele, J.-M., Diot, H., Ennih, N., Plissart, G., Monnier, C., Watlet, A., Bruguier, O., Spagna, P., Vandycke, S., 2016. The Tachakoucht–Iriri–Tourtit arc complex (Moroccan Anti-Atlas): Neoproterozoic records of polyphased subduction-accretion dynamics during the Pan-African orogeny. J. Geodyn. 96, 81–103. https://doi.org/10.1016/j.jog.2015.07.004.

Triantafyllou, A., Berger, J., Baele, J.-M., Bruguier, O., Diot, H., Ennih, N., Monnier, C., Plissart, G., Vandycke, S., Watlet, A., 2018. Intra-oceanic arc growth driven by magmatic and tectonic processes recorded in the Neoproterozoic Bougmane arc complex (Anti-Atlas, Morocco). Precambrian Res. 304, 39–63. https://doi.org/10.1016/j.precamres.2017.10.022.

Triantafyllou, A., Berger, J., Baele, J.M., Mattielli, N., Ducea, M.N., Sterckx, S., Samson, S., Hodel, F., Ennih, N., 2020. Episodic magmatism during the growth of a Neoproterozoic oceanic arc (Anti-Atlas, Morocco). Precambrian Res., 339, 105610. https://doi.org/10.1016/j.precamres.2020.105610

Tshibubudze, A., Hein, K.A.A., McCuaig, T.C., 2015. The relative and absolute chronology of strato-tectonic events in the Gorom-Gorom granitoid terrane and Oudalan-Gorouol belt, northeast Burkina Faso. J. Afr. Earth Sci. 112, 382–418.

Vidal, M., Gumiaux, C., Cagnard, F., Pouclet, A., Ouattara, G., Pichon, M., 2009. Evolution of a Paleoproterozoic “weak type” orogeny in the West African Craton (Ivory Coast). Tectonophysics 477, 145–159.

Walsh, G.J., Aleinikoff, J.N., Benziane, F., Yazidi, A., Armstrong, T.R., 2002. U-Pb zircon geochronology of the Paleoproterozoic Tagragra de Tata inlier and its Neoproterozoic cover, western Anti-Atlas, Morocco. Precambrian Res. 117, 1–20. https://doi.org/10.1016/S0301-9268(02)00044-X

Walsh, G.J., Benziane, F., Aleinikoff, J.N., Harisson, R.W., Yazidi, A., Burton, W.C., Quick, J.E., Saadane, A., 2012. Neoproterozoic tectonic evolution of the Jebel Saghro and Bou Azer-El Graara

1355 inliers, eastern and central Anti-Atlas, Morocco. Precambrian Res. 216-219, 23–62.
1356 https://doi.org/10.1016/j.precamres.2012.06.010
1357 Williams, I.S., 1998. U–Th–Pb geochronology by ion microprobe. In: McKibben, M.A., Shanks III,
1358 W.C., Ridley, W.I. (Eds.), Applications of Microanalytical Techniques to Understanding
1359 Mineralizing Processes, Reviews of Economic Geology 7, 1–35.
1360 Wiedenbeck, M., 1995. An example of reverse discordance during ion microprobe zircon dating: An
1361 artifact of enhanced ion yields from a radiogenic labile Pb. Chemical Geology 125, 197–218.
1362 https://doi.org/10.1016/0009-2541(95)00072-T
1363 Youbi, N., Kouyaté, D., Söderlund, U., Ernst, R.E., Soulaimani, A., Hafid, A., Ikenne, M., El Bahat, A.,
1364 Bertrand, H., Rkha Chaham, K., Ben Abbou, M., Mortaji, A., El Ghorfi, M., Zouhair, M., El Janati,
1365 M., 2013. The 1750 Ma magmatic event of the West African Craton (Anti-Atlas), Morocco.
1366 Precambrian Res. 236, 106–123. https://doi.org/10.1016/j.precamres.2013.07.003

Figures

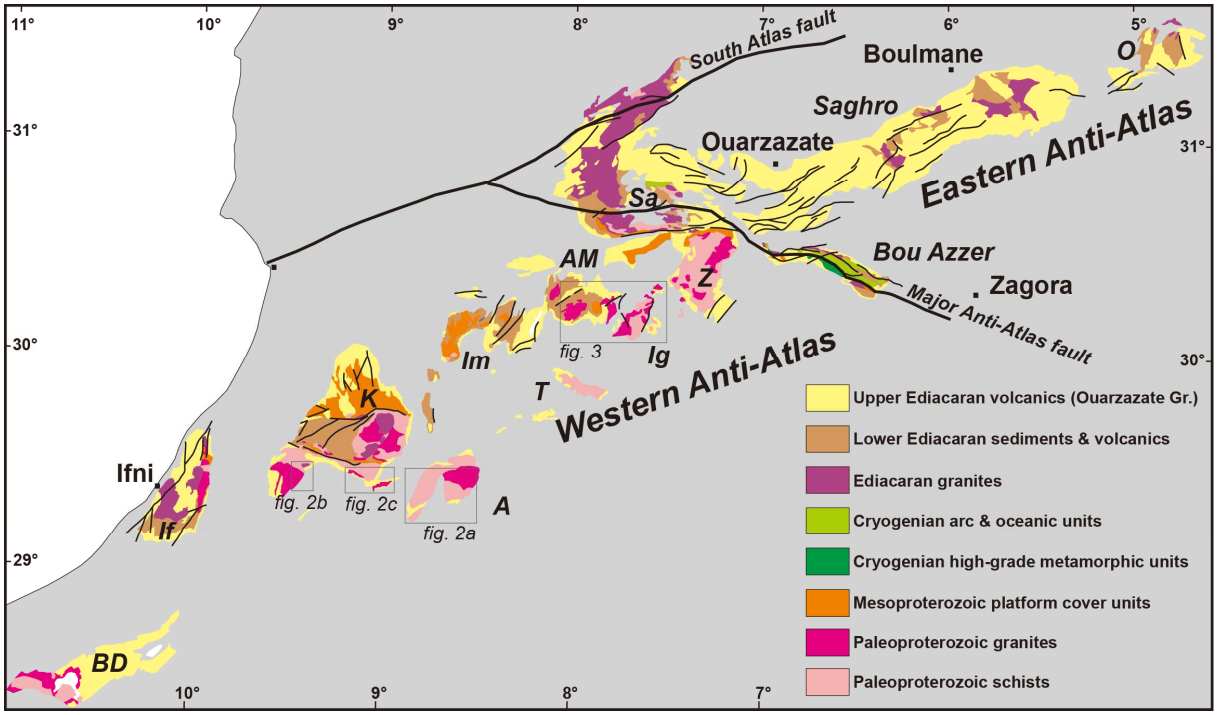

Figure 1: Simplified geologic map of the Anti-Atlas showing the location of the Jebel Saghro and Bou Azzer–El Graara inliers; modified from Hollard et al. (1985), Walsh et al. (2002) and Gasquet et al. (2008). BD: Bas Drâa; If: Ifni; K: Kerdous; A: Tagragra d'Akka; Im: Igherm; T: Tagragra de Tata; Ig: Iguerda; AM: Agadir-Melloul; Sa: Sirwa; O: Ougnat.

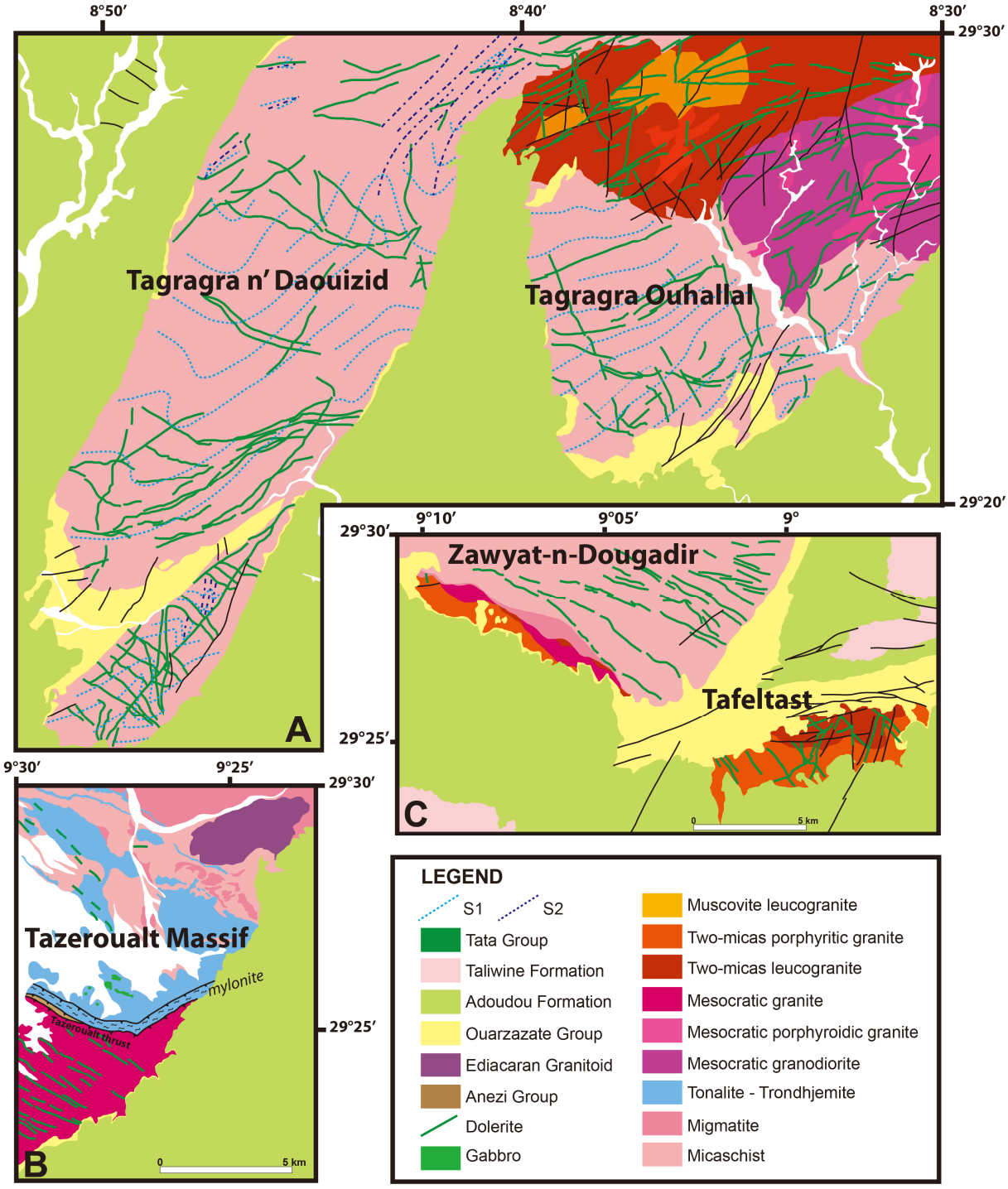

Figure 2: Simplified geologic map of the Tagragra d'Akka inlier (**A**; modified from Roger et al., 2001, and Hassenforder et al., 2001), the Tazeroualt massif (**B**; modified from Calvès et al., 2005), and the Tafeltast massif (**C**; modified from Hassenforder et al., 2001, and Baudin et al., 2005).

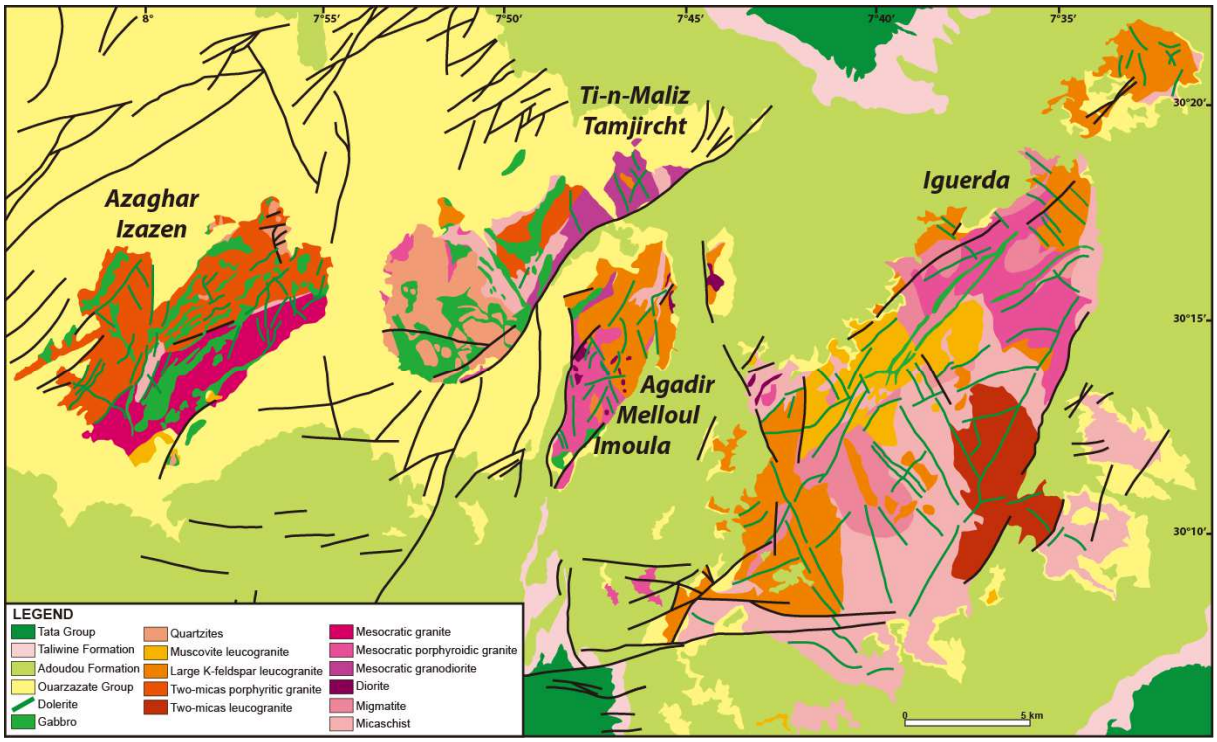

Figure 3: Simplified geologic map of the Iguerda and Agadir-Melloul inliers (modified from Ouanaïmi et al., 2013, Admou et al., 2013, Baudin et al., 2013, and Blein et al., 2013).

1383

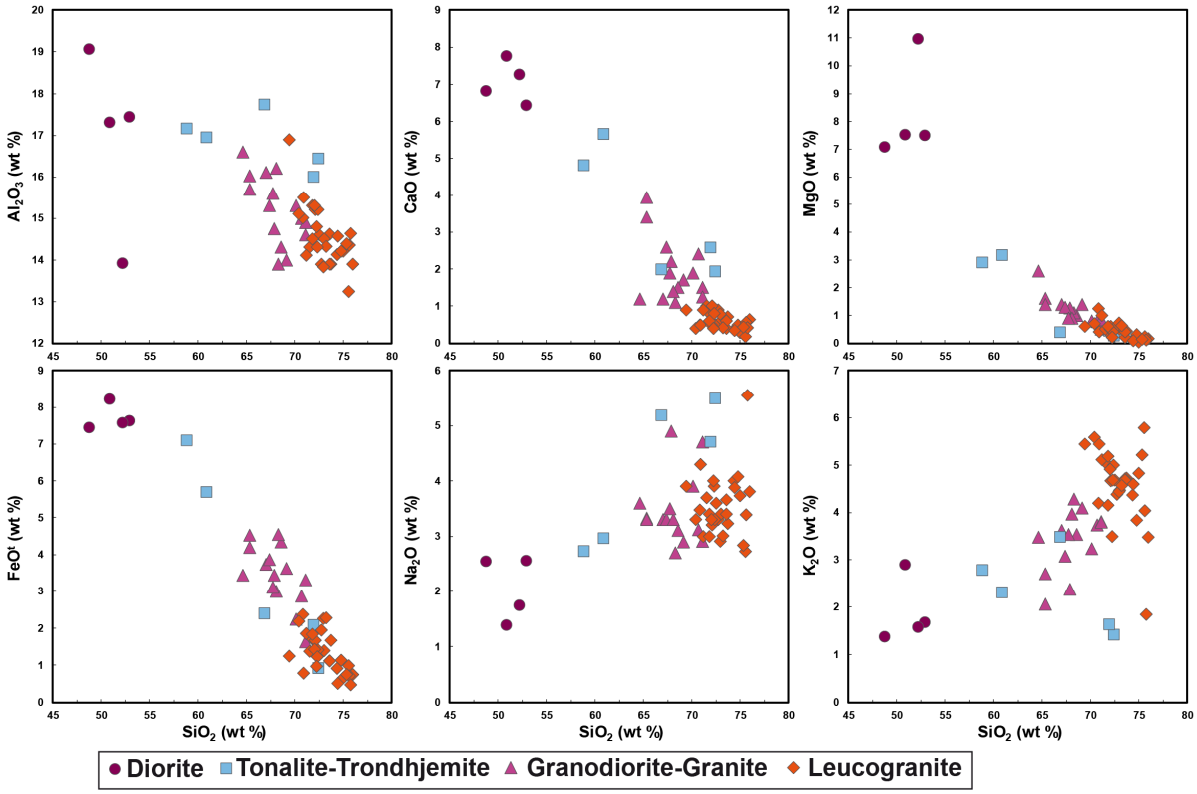

1384

1385 **Figure 4:** Selected Harker plots showing the major element compositions of the Paleoproterozoic

1386 diorites and granites.

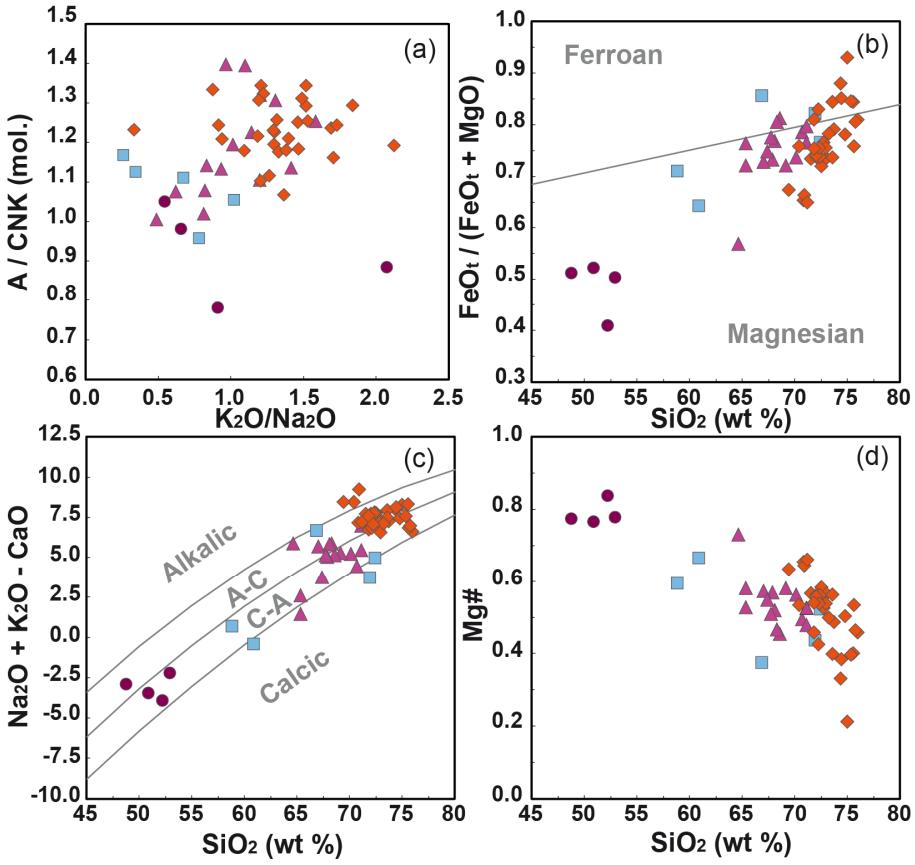

Figure 5: Major-element geochemistry of the Paleoproterozoic diorites and granites (symbols as in Figure 5). (a) A/CNK (molar $Al_2O_3/[CaO + Na_2O + K_2O]$ ratio) vs. K_2O/Na_2O; (b) $FeO^t/(FeO^t + Mg)$ ratio vs. SiO_2. (c) MALI index ($[Na_2O + K_2O] - CaO$) vs SiO_2 diagram of Frost et al. (2001); (d) Mg# vs. SiO_2.

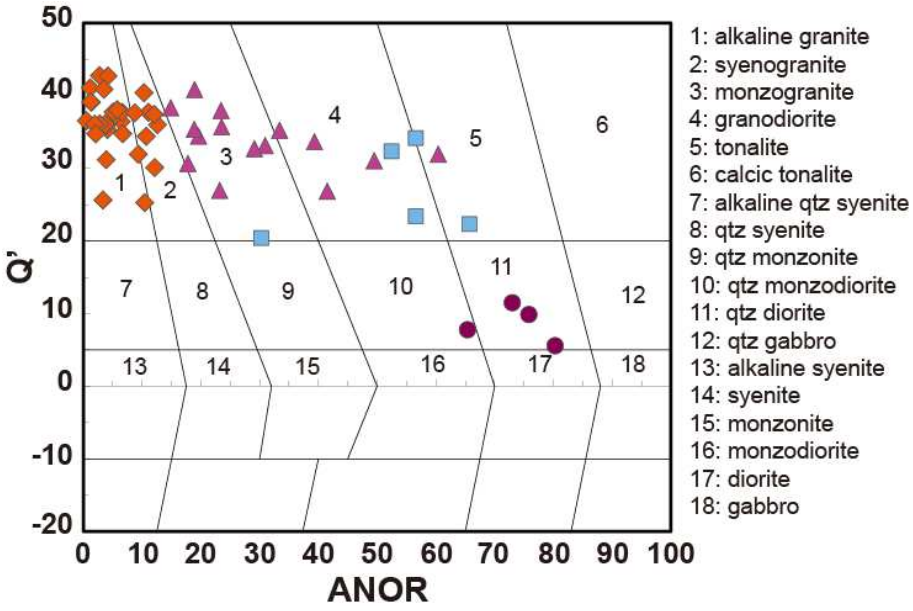

Figure 6: Q' vs. ANOR classification diagram for the Paleoproterozoic diorites and granites (Streckeisen and Le Maître, 1979; symbols as in Figure 4).

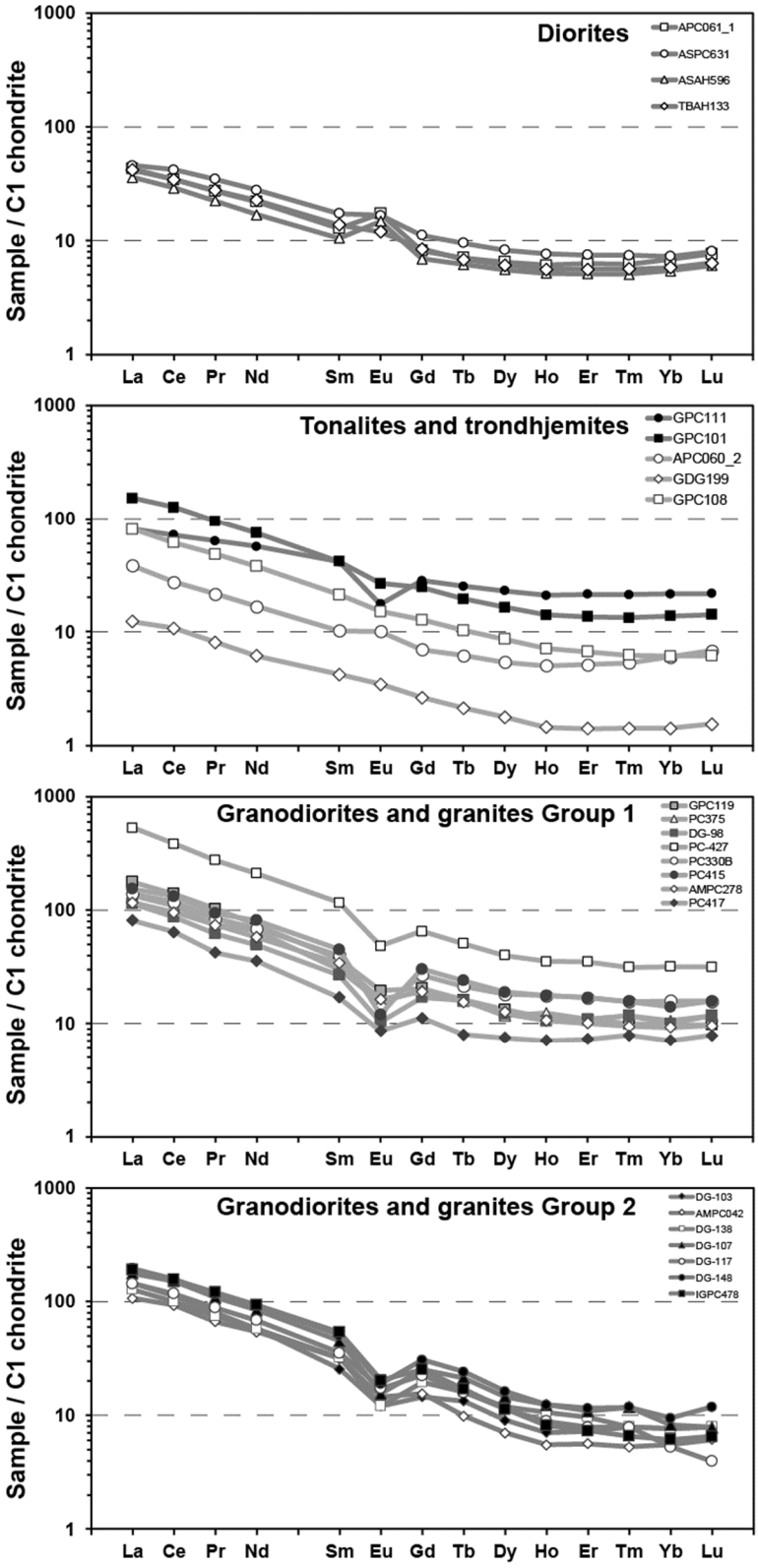

Figure 7: C1 Chondrite-normalized diagrams of Paleoproterozoic diorites and granites of western Anti-Atlas. Normalizing values are from McDonough and Sun (1995).

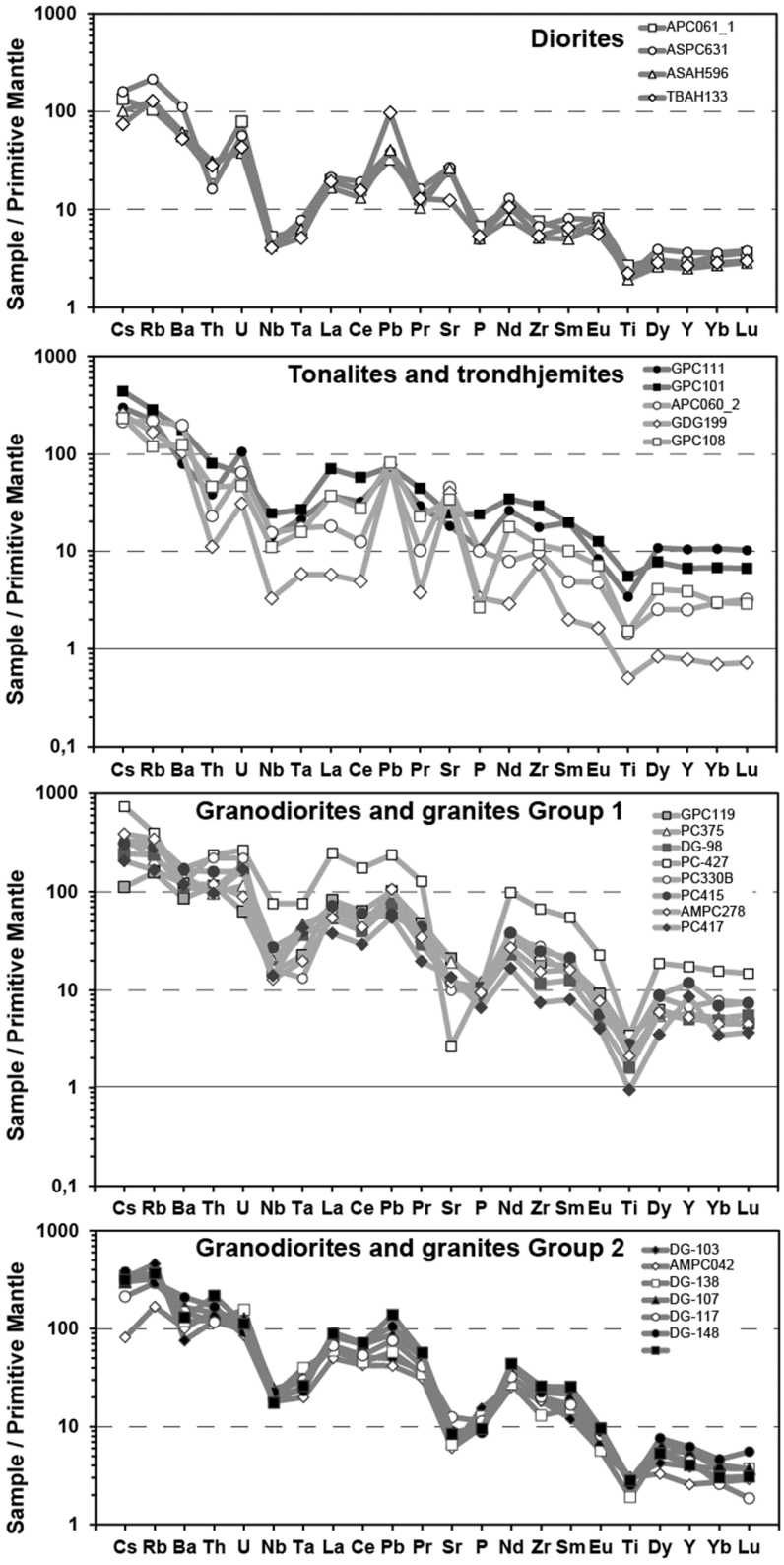

Figure 8: Primitive-mantle-normalized spider diagrams of Paleoproterozoic diorites and granites of western Anti-Atlas. Normalizing values are from McDonough and Sun (1995).

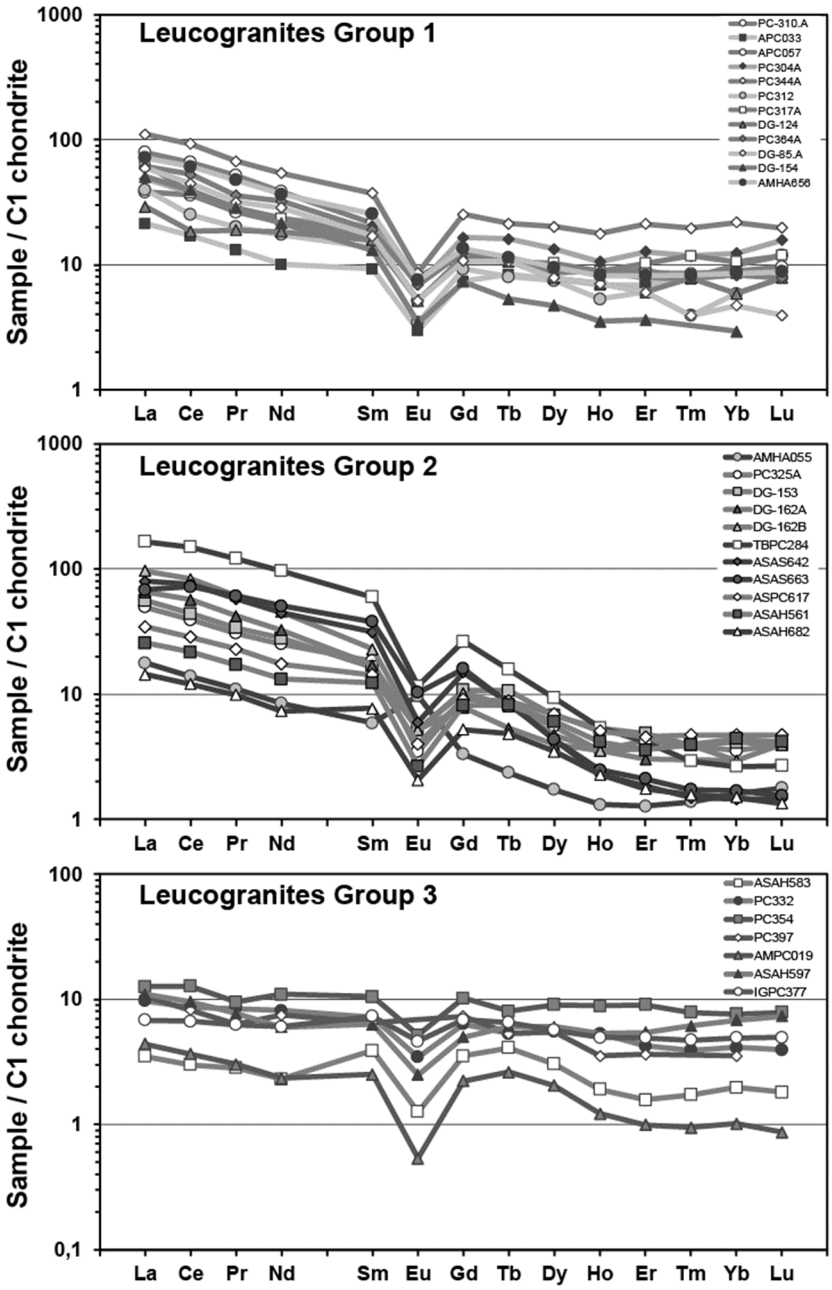

Figure 9: C1 Chondrite normalized diagram of Paleoproterozoic leucogranites of western Anti-Atlas. Normalizing values are from McDonough and Sun (1995).

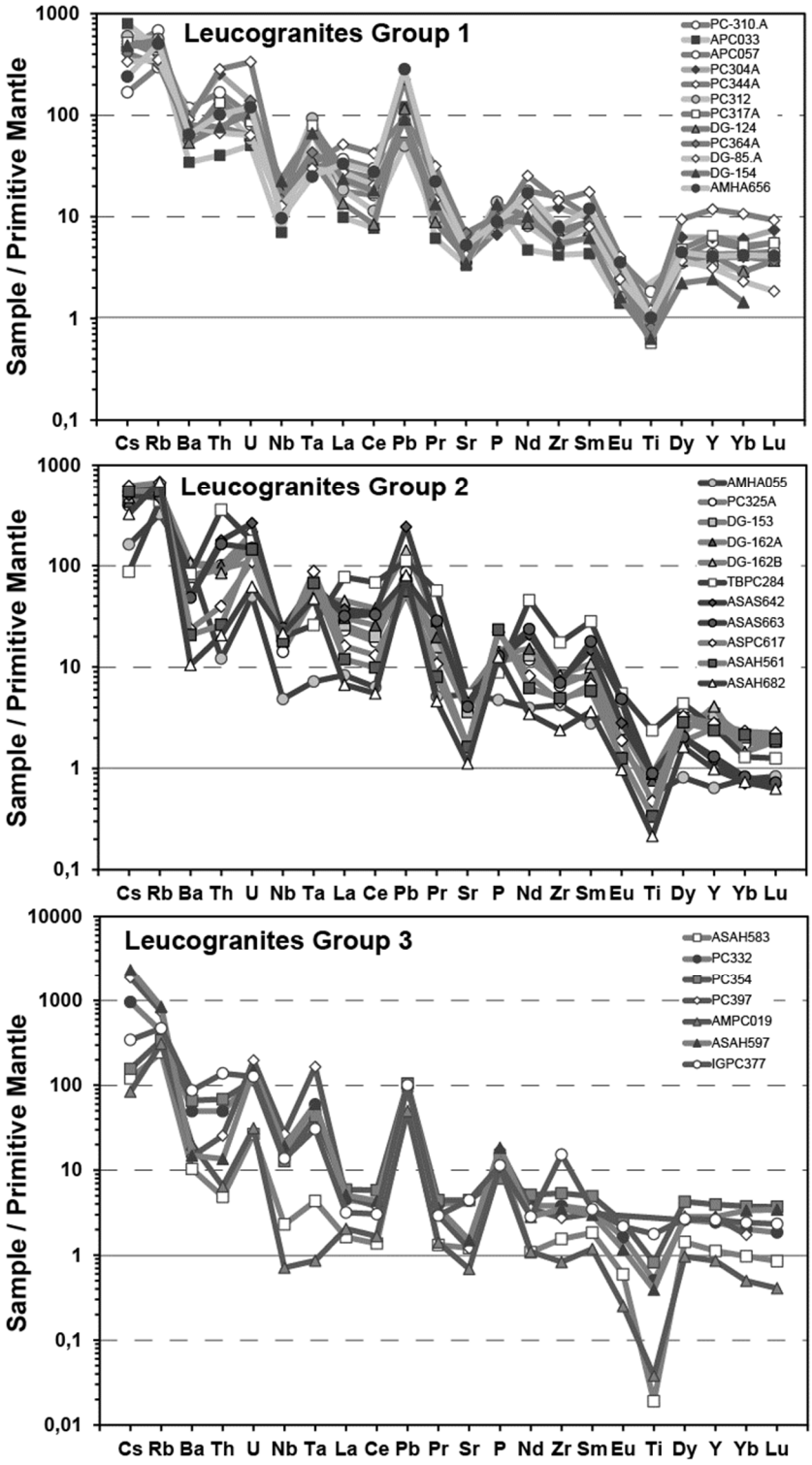

Figure 10: Primitive-mantle-normalized spider diagrams of Paleoproterozoic leucogranites of western Anti-Atlas. Normalizing values are from McDonough and Sun (1995).

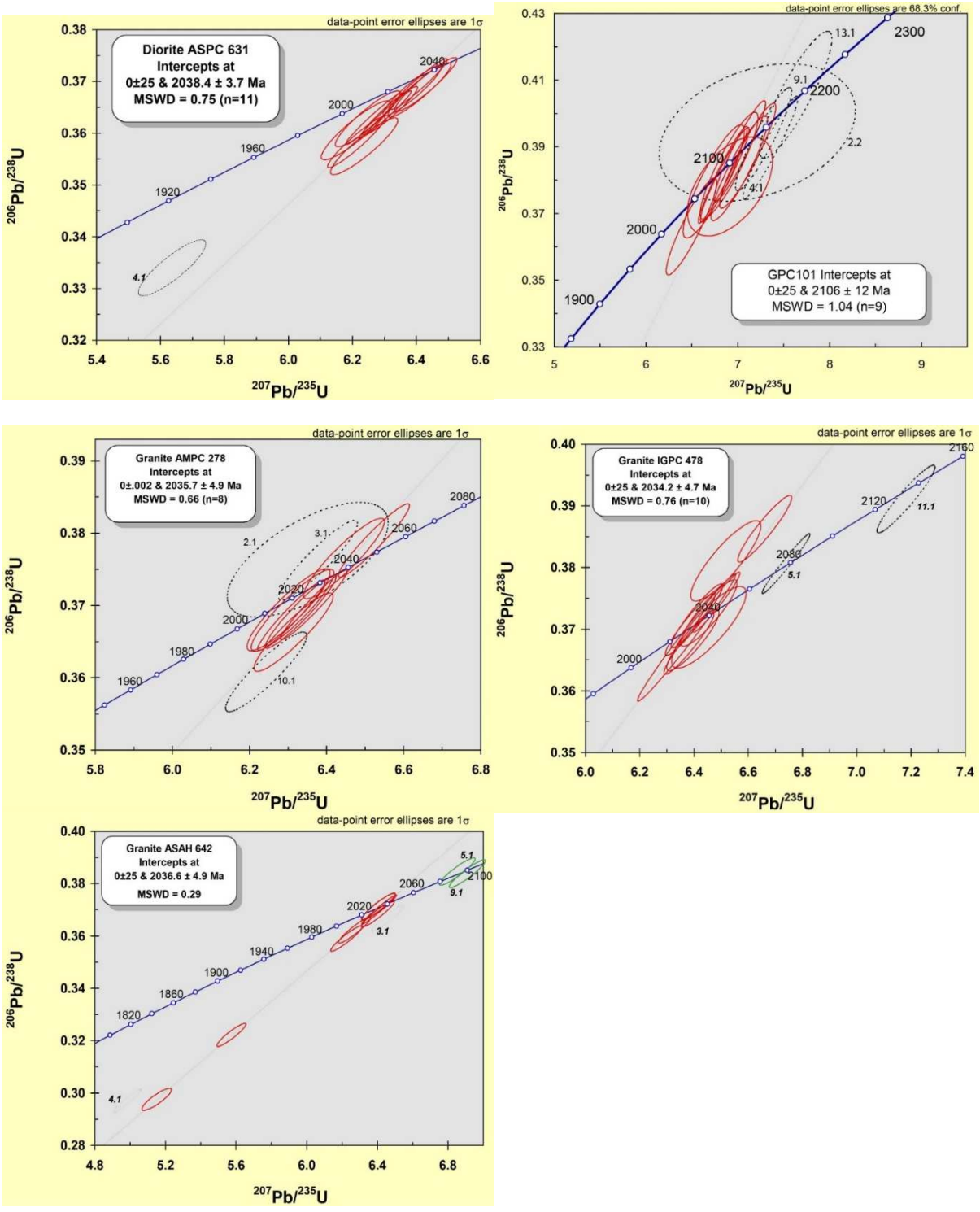

Figure 11: U-Pb concordia diagrams of all analysed zircon grains for a quartz monzodiorite (ASPC631), for a tonalite (GPC101), for a mesocratic granite (AMPC278), for a mesocratic porphyroidic granite (IGPC478), for a two-mica leucogranite (ASAH642).

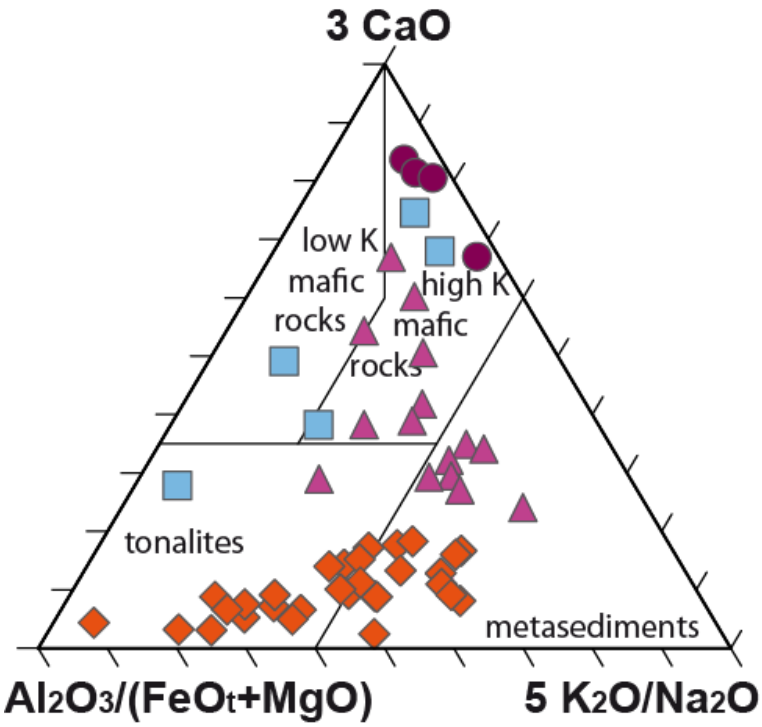

Figure 12: Ternary diagram $Al_2O_3/(FeO^t + MgO)$ - 3 CaO - 5 (K_2O/Na_2O) on which the composition of Paleoproterozoic granitoids from the Anti-Atlas inliers is plotted (symbols as in Figure 12). The fields represent the composition of melts derived from a range of potential sources (tonalites, metasediments, low- and high-K mafic rocks), determined using the major-element compositions of experimental studies (references in Laurent et al., 2014).

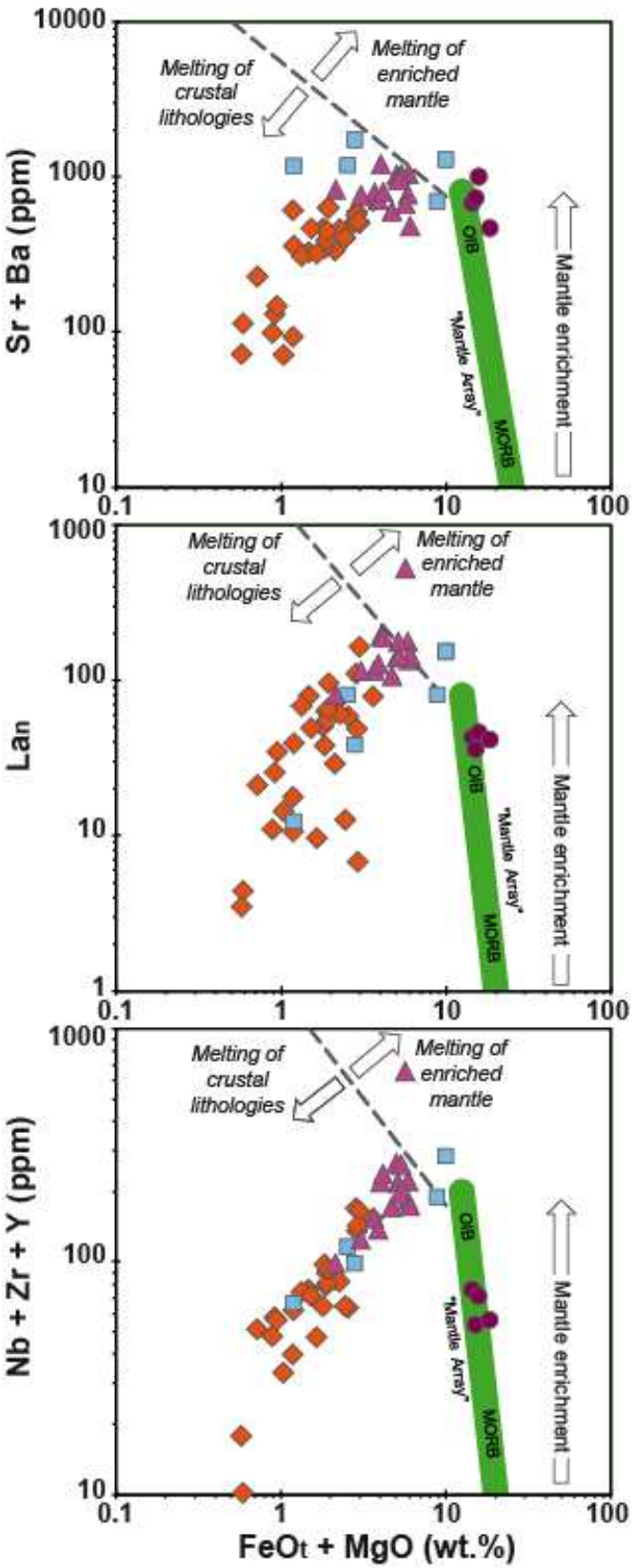

Figure 13: Plots of incompatible element contents (Sr + Ba; La concentrations normalized to C1 chondrite value of McDonough and Sun, 1995; and sum of HFSE = Nb + Zr + Y) plotted as a function of FeO^t + MgO (wt.%) concentrations (symbols as in Figure 12).

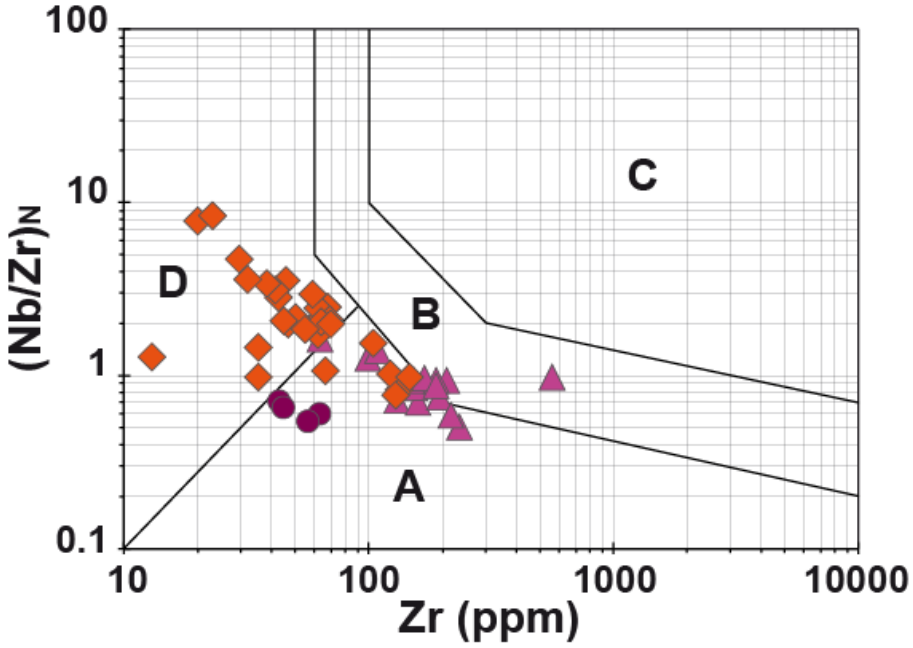

1428

1429 **Figure 14:** Zr vs. $(Nb/Zr)_N$ diagram (Thiéblemont and Tegyey, 1994) for the Paleoproterozoic

1430 granitoids (symbols as in Figure 12).

1431

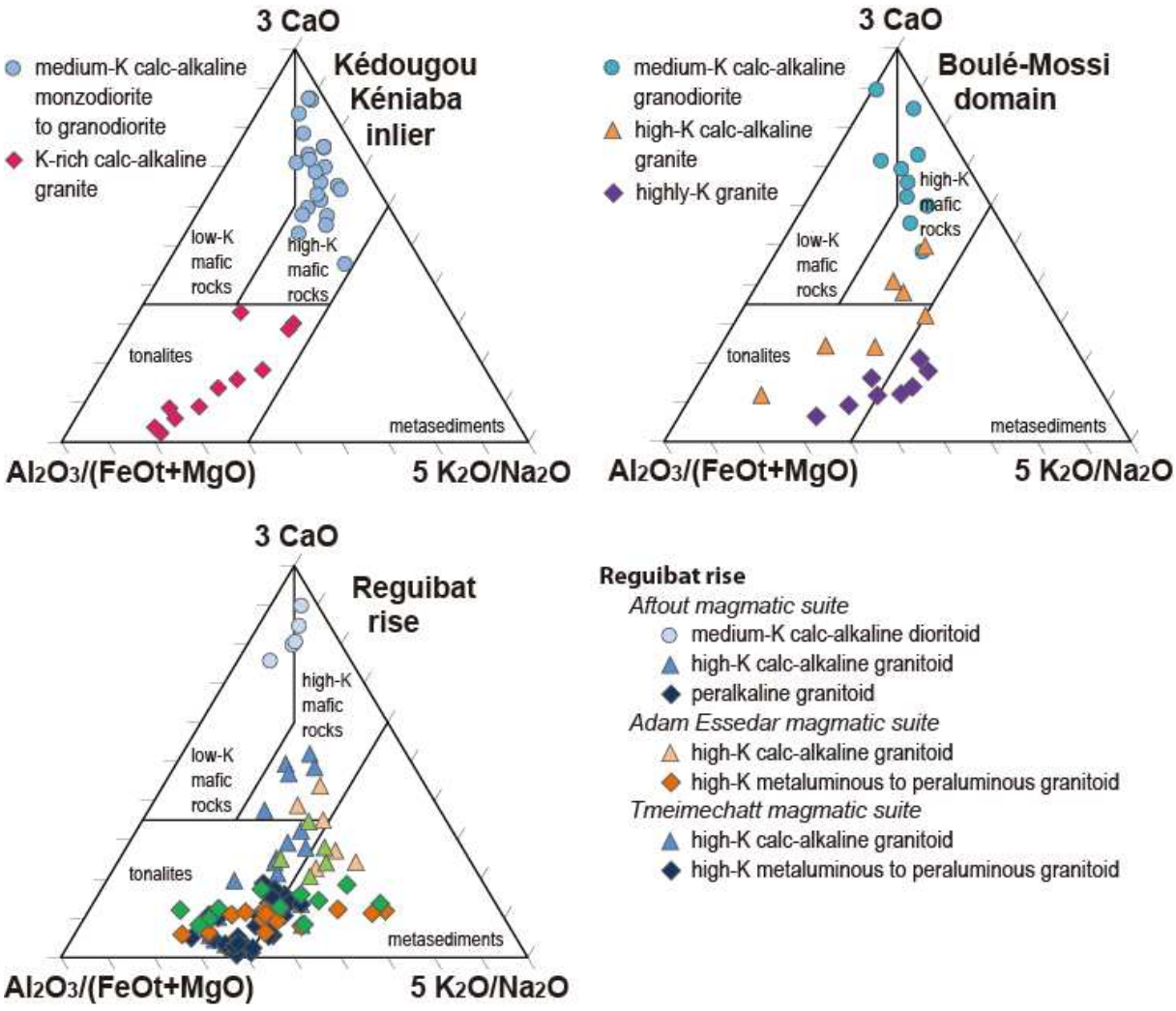

Figure 15: Ternary diagram $Al_2O_3/(FeO^t + MgO)$: 3 CaO; 5 (K_2O/Na_2O) on which the composition of late Eburnean diorites, granodiorites and granites from the Kédougou-Kéniaba inlier, the Boulé-Mossi domain a,d the Reguibat rise is plotted (data from Egal et al., 2002; Lahondère et al., 2003; Peucat et al., 2005; Dioh et al., 2006; Laurent et al., 2014; Masurel et al., 2016).